

Review

# Review of Concentrated Solar Power Technology Applications in Photocatalytic Water Purification and Energy Conversion: Overview, Challenges and Future Directions

Cheng Zhang <sup>1</sup> , Na Li <sup>1</sup> and Guangqi An <sup>2,\*</sup>

<sup>1</sup> National Energy Key Laboratory for New Hydrogen-Ammonia Energy Technologies, Foshan Xianhu Laboratory, Foshan 528200, China; amdain@sina.cn (C.Z.); lina@xhlab.cn (N.L.)

<sup>2</sup> Graduate School of Life and Environmental Science, University of Tsukuba, 1-1-1 Tennodai, Tsukuba 305-8572, Ibaraki, Japan

\* Correspondence: s2236023@u.tsukuba.ac.jp; Tel./Fax: +81-070-3145-8576

**Abstract:** Photocatalysis, a promising semiconductor-based technology activated by free and eternal solar energy, has great potential for addressing environmental remediation and energy conversion challenges. Concentrated solar power (CSP) technologies, namely parabolic trough reflectors, solar power towers, parabolic dish reflectors and linear Fresnel reflectors, exhibited excellent feasibility for boosting solar-driven photocatalytic processes. Based on the structural characteristics of CSP technologies, the CSP-based photocatalytic reactors could be divided into concentrated types and non/low-concentrated types. This academic review comprehensively investigated the integration of CSP technology in photocatalysis, emphasizing the feasibility of sunlight as an ideal energy source. Additionally, considering the optimal light irradiance and reaction temperature demands for achieving efficient photocatalytic processes, the significance of introducing CSP into solar light-driven photocatalytic reactions was highlighted. Moreover, the current challenges that exist in CSP-based photoreactors were identified, and potential solutions were proposed accordingly. This work hopes to provide some references for the future study of CSP-based photocatalytic reactors under the theme of sustainable development.

**Keywords:** concentrated solar power (CSP) technology; photocatalysis; solar energy; photoreactor; sustainable development



**Citation:** Zhang, C.; Li, N.; An, G. Review of Concentrated Solar Power Technology Applications in Photocatalytic Water Purification and Energy Conversion: Overview, Challenges and Future Directions. *Energies* **2024**, *17*, 463. <https://doi.org/10.3390/en17020463>

Academic Editor: Carlo Renno

Received: 20 December 2023

Revised: 12 January 2024

Accepted: 15 January 2024

Published: 18 January 2024



**Copyright:** © 2024 by the authors. Licensee MDPI, Basel, Switzerland. This article is an open access article distributed under the terms and conditions of the Creative Commons Attribution (CC BY) license (<https://creativecommons.org/licenses/by/4.0/>).

## 1. Introduction

The sustainable development of the global economy and society is being disrupted by environmental deterioration, energy crises and other aspects [1]. The traditional way of production and life requires a large amount of non-renewable energy to drive, which not only further aggravates the problem of insufficient energy supply but also continues to destroy the ecological environment. Faced with this dilemma, the United Nations put forward the Sustainable Development Goals (SDGs), which emphasize the utilization of renewable energy and new production development modes [2]. Motivated by this, significant effort has been put into searching for new process strategies for energy conservation and emission reduction and studying their utilization patterns.

In the last few decades, photocatalysis has been intensively studied [3–5]. Under the illumination of incident light, the photocatalyst, as a semiconductor, could be excited to release electrons and holes, thereby leading to the subsequent generation of free radicals (such as superoxide radicals, hydroxyl radicals, etc.) with strong oxidation–reducing properties [6]. These free radicals could act on the structure of organic molecules and destroy their molecular bonds, resulting in the destruction and degradation of organic particles with no change occurring on the photocatalyst itself. Owing to the non-selectivity, cost-effectiveness,

non-toxicity and eco-friendliness, photocatalytic technology exhibited impressive application potential in environment remediation (e.g., wastewater treatment [7,8], abatement of noxious gases [9], sterilization ([3,10], etc.), energy conversion (e.g., water splitting for hydrogen generation [11,12], hydrogen formation via ammonia decomposition [13,14], microalgae biorefinery [1], etc.) and so on. In order to boost this promising technology further into practical applications, the sources of energy used to drive photocatalytic reactions need to be carefully selected. Solar energy, as a natural source of light, has the following exciting characteristics: (1) permanent supply of energy, (2) wide distribution on earth, (3) easy utilization availability and (4) wide spectral band of wavelengths. Although the proportion of high-energy UV photons is only 3% to 5% of the total solar energy, it does not affect solar light to be the ideal driving force to motivate the photocatalytic processes [1,3,4,7].

As a bridge between sources of driving forces (solar energy) and users of driving forces (photocatalysis), photocatalytic reactors have been studied tirelessly in recent decades. The simplest photoreactor was a beaker placed under simulated solar light irradiation, which was filled with a photocatalyst and reactant [15,16]. Despite initiating the photocatalytic reaction, it was obviously far from practical application. Going one step further, some primitive but systematic prototype photoreactors have been developed and studied, including the classic inclined plate reactor (IPR) [7]. The structure of an IPR is characterized by an inclined plane facing the direction of solar light incidence, and the angle of inclination can be adjusted according to the local latitude. The photocatalyst is immobilized or flows down with wastewater in powder form, and the photocatalytic process is implemented upon the inclined plate. This simple and inexpensive design propelled IPR into widespread use, and an IPR-based wastewater treatment plant was even manufactured for purifying industrial wastewater from textile mills [17]. Nevertheless, one obvious disadvantage of IPR is that it leads to insufficient photocatalytic activity because of the low solar energy collecting efficiency brought on by passive acceptance of solar light [7]. Aiming to promote photocatalytic efficiency under actual sunlight, new photoreactor concepts are required. When it comes to effectively harvesting sunlight, it is natural to think of concentrated solar power (CSP) technology. CSP technology refers to the renewable energy project that concentrates, collects and converts solar energy into heat flux through a photo-thermal conversion process [18]. It has attracted great attention, owing to its unique advantages such as its superior capability for light and thermal collection, wide feasibility for multiple utilization purposes and high technical maturity. Generally, CSP technology can be divided into parabolic trough reflectors (PTRs), solar power towers (SPTs), parabolic dish reflectors (PDRs) and linear Fresnel reflectors (LFRs) according to their system configurations [19]. Since the effective solar energy collection capability of CSP technology matches the demand for solar energy-driven photocatalytic processes, it is not surprising that CSP-based photoreactors are widely developed and studied.

Based on the above background, this academic review is dedicated to demonstrating the integration and application of CSP technology in photocatalytic processes, especially water purification and energy conversion. Preferentially, the principle of the action between solar energy and photocatalysis is explained, and the legitimacy and rationality of sunlight as an ideal light source for photocatalysis is highlighted. Then, the reasons why CSP technology is meaningful and necessary to be introduced into solar energy-driven photocatalytic reactions is explained from the perspective of energy demand for efficient photocatalysis. Subsequently, four typical CSP configurations (including PTR, SPT, PDR and LFR), as well as their traditional applications, are described. In addition, as the highlight of this review, the original idea, development process, current status and future research trends of each CSP-based photocatalytic reactor are emphatically introduced. In this section, CSP-based photocatalytic photoreactors are classified as solar-concentrated types and solar non/low-concentrated types according to their solar concentration ratio, which will be introduced in order to present the technological changes. Moreover, some of the state-of-art photocatalytic reactor technologies, such as solar energy control strategies and 24 h all-weather systems, will also be demonstrated. Furthermore, the current chal-

allenges faced by CSP-based photocatalytic reactors are also pointed out, and some potential ideas for solving these problems are provided.

## 2. Feasibility of Solar Energy for Photocatalytic Applications

The formation of electrons and holes in photocatalysts requires photon excitation with sufficient energy. In order to excite electrons from the valence band (VB) of the photocatalyst to the conduction band (CB), the photon energy carried by the incident light needs to overcome the band gap between the VB and CB (as shown in Figure 1a). After decades of development, a large family of photocatalysts has been formed. According to the element composition, synthesis conditions and defect location, different photocatalysts have different band gaps. Figure 1b shows the light wavelength required for activating some typical photocatalysts (data from [8,20–37]). It can be seen that although the sun emits light over a wide range of wavelengths, traditional photocatalysts such as  $\text{TiO}_2$  can only be excited by UV light with wavelengths less than 380 nm [28]. Since UV energy only accounts for a small proportion of solar energy, this results in low UV radiation intensity and low photocatalytic efficiency. In recent years, newly developed photocatalysts such as P/Ag/Ag<sub>2</sub>O/Ag<sub>3</sub>PO<sub>4</sub>/TiO<sub>2</sub> composites [31] have expanded the utilizable solar radiation band, enabling it to be excited by both visible light and UV, significantly improving the photocatalytic efficiency compared to  $\text{TiO}_2$  alone. Since solar energy is an infinite and widely distributed light source possessing a broad spectrum wavelength ranging from 300 to 2500 nm [7], it could excite the photocatalyst with any band gap, thus implementing the photocatalytic reaction process.

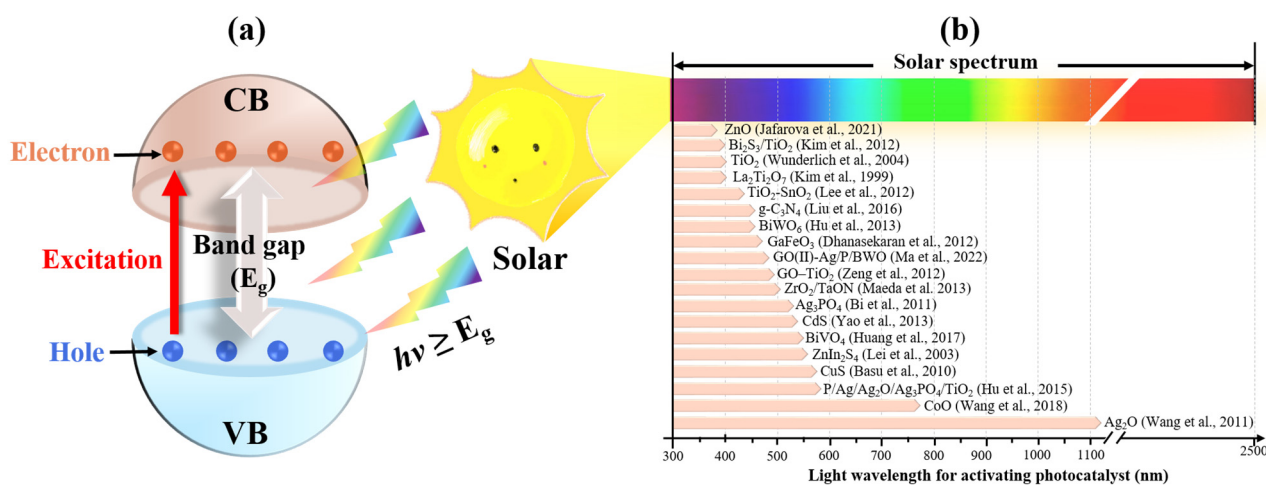


**Figure 1.** Activation of photocatalysts under solar light. (a) Generation of electron and hole; (b) light wavelength required for activating different photocatalysts [8,20–37].

In addition, from a practical point of view, to make photocatalytic technology applicable, efficient photocatalytic processes need to be pursued. Therefore, suitable photocatalytic reaction conditions need to be provided and maintained. Since solar light energy mainly provides light irradiance and the reaction temperature, whether natural sunlight is qualified to meet the appropriate reaction conditions for efficient photocatalysis needs to be investigated. Figure 2a illustrates the optimal light irradiance required for various photocatalytic reactions. It can be observed that for a wide range of photocatalytic reactions, including the removal of organic dyes (rhodamine b, tartrazine, reactive black 5, etc.) [7,38,39], the degradation of harmful antibiotics (metronidazole, tetracycline, cephalexin, etc.) [40,41], the inactivation of pathogenic bacteria (*Escherichia coli*, etc.) [42] and the oxidation of organic matters (aerobic oxidation, etc.) [43], the light irradiance in the range of 600–1600 W/m<sup>2</sup> is conducive to the implementation of efficient photocatalytic reactions (Figure 2a). However, under real environmental conditions, the solar light irradiance (data from [7,44–49]) is much lower than the appropriate light irradiance required for efficient photocatalysis

(Figure 2a). For example, Basem et al. reported that the maximum sunlight irradiance on a typical sunny day (during December) in Iraq was only  $500 \text{ W/m}^2$  [49]. Additionally, Cao et al. measured the annual solar irradiance in Northwest China and found that the average value was  $641 \text{ W/m}^2$  [48]. Moreover, Zhang et al. investigated the whole-year solar light irradiance in Japan, which ranged from  $0\text{--}767 \text{ W/m}^2$  for Tsukuba ( $36.1^\circ \text{ N}$ ) and  $0\text{--}633 \text{ W/m}^2$  for Sapporo ( $43.4^\circ \text{ N}$ ) [7]. Since Tsukuba-Sapporo is located in Japan's latitude zone, which is the latitude range with the most densely populated areas in the world [7], the natural solar irradiance of most of the world can also be inferred to be within  $800 \text{ W/m}^2$ . Therefore, natural solar light irradiance needs to be enhanced to meet the needs of efficient photocatalytic reactions.

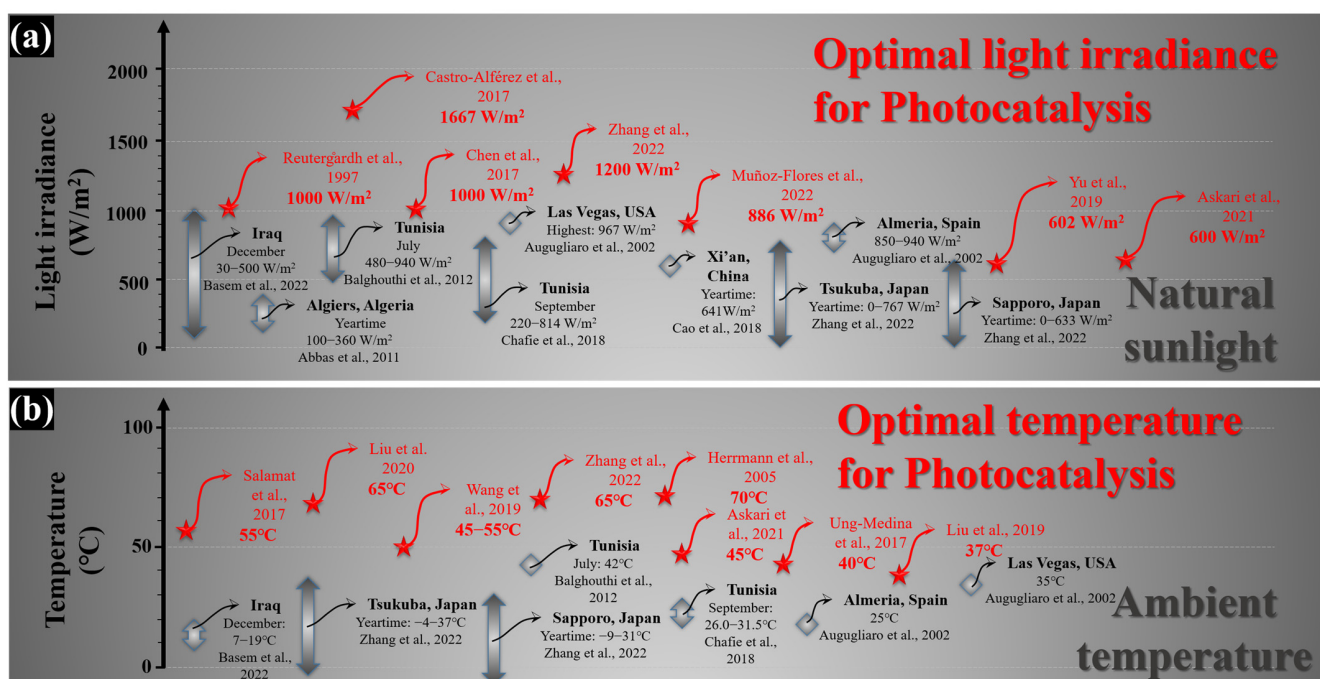


**Figure 2.** Comparison of optimum photocatalytic reaction conditions with natural conditions. (a) Light irradiance [7,38–49]; (b) temperature [7,10,40,45–47,49–54].

On the other hand, in order to further investigate whether natural solar energy is qualified to support efficient photocatalytic reactions, a comparison between ambient temperature and the favorable reaction temperature was carried out. As shown in Figure 2b, a wide range of photocatalytic reactions, including the treatment of steel mill wastewater [51], organic wastewater treatment (containing acid blue 9 or rhodamine b) [7,54], sterilization (*Escherichia coli*, etc.) [10], treatment of harmful antibiotics (cephalexin, metronidazole, tetracycline, etc.) [40,53] and oxidation of acetone [52], require a suitable reaction temperature ranging from 37 to  $70^\circ \text{C}$  for maximizing their efficiency (Figure 2b). In addition, the influence of the reaction temperature on the kinetics of photocatalysis was also studied, which indicated that  $70^\circ \text{C}$  might be a superior temperature for maximizing photocatalytic efficiency [50]. However, many researchers have reported their local ambient temperature, confirming that ambient temperatures directly converted by natural sunlight may not be conducive to efficient photocatalytic reactions (Figure 2b). For example, November temperatures in Iraq ranged from  $7.0\text{--}19.0^\circ \text{C}$  [49], September temperatures in Tunisia ranged from  $26.0\text{--}31.5^\circ \text{C}$  [47], a typical sunny day in Las Vegas in the US was approximately  $35.0^\circ \text{C}$  [46] and year-round temperatures in Tsukuba and Sapporo in Japan ranged from  $-4.0$  to  $37.0^\circ \text{C}$  and  $-9.0$  to  $31.0^\circ \text{C}$ , respectively [7]. Although solar energy could effectively initiate photocatalytic reactions, its inherent low energy density makes it difficult to achieve optimal photocatalytic efficiency when using sunlight directly. Hence, to boost the photocatalytic reaction efficiency by adopting free and eternal solar energy, sunlight needs

to be concentrated. CSP technology, an effective approach for solar energy convergence, could have significant advantages in meeting this demand.

### 3. Brief Overview of Concentrated Solar Power Technologies

The history of CSP probably dates back to the beginning of attempts to harness photo-thermal energy. As technology continues to advance, CSP design and manufacturing techniques continue to improve. With the development of materials science and manufacturing processes, people began to use more durable and more reflective materials to create CSP. In the past decades, with the increasingly prominent energy crisis and environmental problems, solar energy technology has become more widely used and researched. During this period, CSP design and manufacturing techniques were further improved. For example, computer-aided design (CAD) and optical techniques are being used to optimize the structure and reflection properties of solar technologies, and applications of novel materials and manufacturing processes are being explored. Currently, according to the configuration characteristics, CSP can be classified as PTR, PDR, SPT and LFR.

#### 3.1. Parabolic Trough Reflectors

The PTR might be the most common and widely deployed CSP technology. As shown in Figure 3a, the most important technical feature of the PTR is that it is equipped with a parabolic-shaped concentrator mirror and a receiver tube located at the focal line of the parabola [45]. Owing to the optical properties of the paraboloid, it can efficiently focus incident parallel sunlight onto its focal line. This capability allows the receiver to harness a substantial amount of light energy, subsequently converting it into a concentrated heat flux. In order for the parabolic mirror to accurately converge parallel solar rays, the aperture of the parabola must always face the incidence direction of sunlight accurately. Therefore, parabolic mirrors are usually equipped with a controlling system to track solar motion. Due to its simpler structure compared with other CSP technologies, PTR has been successfully applied in various application scenarios. The most interesting application of PTR might be in the field of solar thermal power generation [55]. By concentrating a large amount of light and heat energy, the thermal medium (such as thermal oil and molten salts) in the receiver tube is heated, thus heating the water into high-temperature steam, which drives the turbine to generate electricity. Additionally, the solar cooking system also consists of an aluminum reflector with a vacuum tube, which provides a suitable cooking temperature of over 200 °C under actual solar conditions [56]. Moreover, the systems employed for desalination were also established by combining the PTR with an evacuated tube [57]. Furthermore, a PTR-based solar adsorption refrigeration system was also investigated, which used olive waste as the adsorbent and methanol as the adsorbate [58]. Other applications of PTR include but are not limited to photo-thermal direct sterilization systems [59], photoelectrochemical reactors for contaminant removal [60], photo-Fenton reactors [61] and industrial process heat [62]. These applications demonstrate the wide applicability and flexible deployability of PTR technology.

#### 3.2. Parabolic Dish Reflectors

The main components of a PDR system (shown in Figure 3b) include a parabolic dish concentrator mirror and a thermal receiver mounted at the focus point of the parabolic dish [63]. Similar to PTR technology, PDR also requires the incident direction of the parallel sunlight to be perpendicular to the aperture of the parabolic dish, thus enabling effective solar energy harvesting. Therefore, a two-axis sun tracking system is also indispensable for PDR. Generally, PDR systems are characterized by a high efficiency, autonomous operation and excellent modularity [63]. Many PDR-based power plants have been manufactured worldwide, which exhibit high solar-to-electric conversion efficiency and have the potential to become one of the most effective renewable energy utilization approaches [44,49,63]. Additionally, owing to their inherent simplicity, portability and cost-effectiveness, solar cooker systems are also regarded as one of the most significant application fields of

PDR [64–66]. Moreover, the solar desalination system based on PDR was also experimentally tested, in which a triple basin glass solar still was fabricated and located upon the focus point of the parabola dish for adsorbing solar energy [67]. Therefore, PDR systems also share merits for wide deployment in different fields to achieve multiple goals.

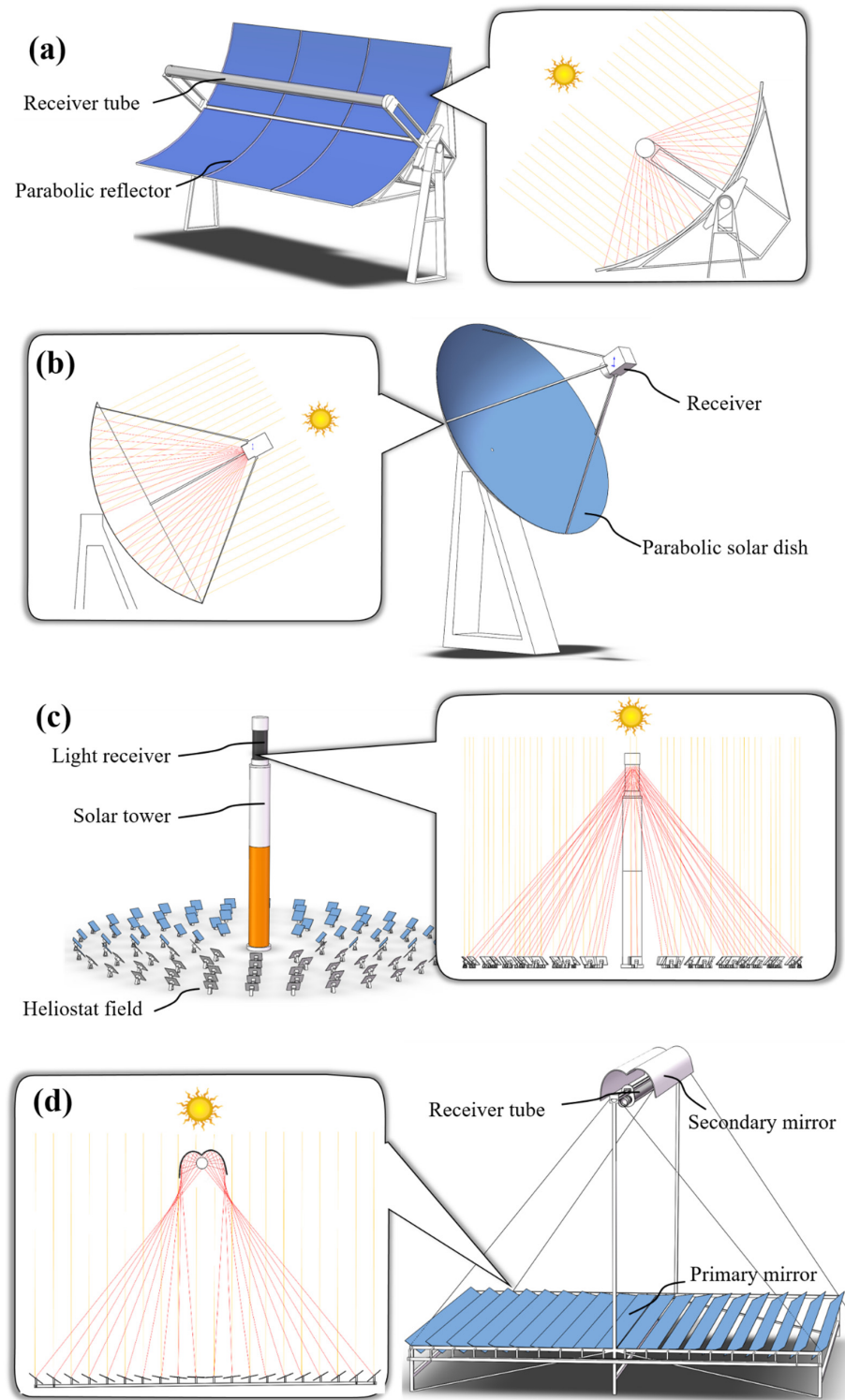


**Figure 3.** Schematic diagram of major concentrated solar power (CSP) technologies. (a) Parabolic trough reflector (PTR); (b) parabolic dish reflector (PDR); (c) solar power tower (SPT) and (d) linear Fresnel reflector (LFR).

### 3.3. Solar Power Towers

In recent decades, as a representative of high-temperature concentration engineering, SPT has been a popular topic in CSP engineering applications [68]. As shown in Figure 3c, in the SPT system, a large number of heliostats are arranged in an oval shape around the heat collecting tower. The heliostat could automatically track the movement of the sun and focus sunlight to the receiver located above the tower, thereby converting light energy into heat flux. The solar concentration ratio of a SPT can reach the equivalent of hundreds to thousands of suns, thereby achieving ultra-high operating temperatures. In recent years, to achieve the goal of saving energy and reducing emissions, SPT-based photo-thermal power plants employing the Rankine or Brayton cycle have been intensively studied and deployed [69]. The above deployment and operation of SPT power plants demonstrates their excellent availability and realizability in solar energy collection.

### 3.4. Linear Fresnel Reflectors

In the past few decades, LFRs have also been studied and developed, and they have been widely used in photo-thermal power generation projects [70,71]. As shown in Figure 3d, the main structure of an LFR includes segmented flat mirrors which are mounted in parallel (as a primary mirror) and a secondary mirror located above the primary mirror array. The light receiver is mounted at the focus position of the secondary mirror. Each row of primary mirrors has a rotation axis, and all the primary mirrors track the position of the sun in the sky under the control of the driving mechanism, focusing the sunlight on the secondary mirror [7]. The shape of the secondary mirror is a compound parabolic collector (CPC) that can capture and reflect incoming sunlight in all directions to its focal point [72]. CPC, as a supporting CSP technology for LFR, plays a crucial role in improving the efficiency and heat flow uniformity of LFR systems. CPC is usually formed by a variety of shape combinations (such as involute, parabola, etc.), thus endowing it with the unique capability to collect beam radiation and diffuse radiation within a specific acceptable half-angle and without the utilization of a complex solar tracking system [73]. Owing to the cooperation of the primary mirror and secondary mirror (CPC), the heat flux could be distributed uniformly over the receiver's surface, thus enabling the achievement of a high thermal efficiency in LFR systems. Usually, LFR can reach a solar concentrating ratio equivalent to tens to hundreds of suns, thereby achieving an operating temperature of 500 °C [29,71]. Due to the low cost of flat primary mirrors and single-axis control systems, LFRs are generally considered to have superior economic efficiency for solar energy collection [7].

## 4. CSP Technologies Applied in Photocatalysis

To effectively provide solar energy for photocatalytic reactions, a large amount of photocatalytic reactors have been designed and developed. Due to the excellent performance of CSP technology in harvesting solar light energy and heat energy conversion, it is naturally applied as the design basis of photocatalytic reactors. As shown in Table 1, according to the structure of the solar concentrator, these photoreactors could be classified into PTR, PDR, LFR, FL, V-groove and CPC, which are organized in a timeline. Reviewing the past photocatalytic reactors based on CSP technology, they can be further divided into solar concentrated types and solar non/low-concentrated types, which are depicted below.

Table 1. Summary of photocatalytic reactors employing CSP technology.

Thematic Axis of Reactor	Dimension of Sunlight Reflector	Reactant Volume	Temperature	Irradiance	Deployed Location	Photocatalyst	Treatment Target	Timeline	Ref.
PTR	-	-	-	-	U.S. (latitude: 38.6° N)	TiO <sub>2</sub>	Groundwater	1991	[74]
	Width: 1.8 m; Length: 4.5 m	-	-	-	Spain (latitude: 37.4° N)	TiO <sub>2</sub>	Pentachlorophenol	1993	[75]
	Width: 1.8 m; Length: 4.5 m	220 L	-	-	Spain (latitude: 37.4° N)	TiO <sub>2</sub>	Atrazine	1996	[75]
	29.1 m <sup>2</sup>	260 L	-	-	Spain (latitude: 37.4° N)	TiO <sub>2</sub>	2,4-Dichlorophenol	1997	[76]
	-	80 L	-	-	Germany (latitude: 50.6° N)	TiO <sub>2</sub>	C <sub>2</sub> H <sub>5</sub> NH <sub>2</sub> and (C <sub>2</sub> H <sub>5</sub> ) <sub>2</sub> NH	2000	[77]
	Width: 1 m; Length: 1 m	-	200–250 °C	-	Japan (latitude: 36° N)	Pt-TiO <sub>2</sub>	Toluene, acetaldehyde	2004	[78]
	0.72 m <sup>2</sup>	10 L	-	-	Mexico (latitude: 19° N)	TiO <sub>2</sub>	Oxalic acid	2004	[79]
	0.042 m <sup>2</sup>	1 L	<38 °C	-	Spain (latitude: 37° N)	TiO <sub>2</sub>	<i>Escherichia coli</i>	2004	[80]
Width: 0.5 m; Length: 1.4 m	-	-	-	Iran (latitude: 22.4° N)	g-C <sub>3</sub> N <sub>4</sub> /TiO <sub>2</sub>	Methylene blue and rhodamine b	2021	[81]	
PDR	0.785 m <sup>2</sup>	3 L	30–58 °C	10–35 W/m <sup>2</sup> (UV)	Japan (latitude: 35.4° N)	TiO <sub>2</sub>	Detergent	2004	[82]
LFR	Width: 0.055 m; Length: 0.23 m	1 L	≤52 °C	24–40 W/m <sup>2</sup> (UV)	Japan (latitude: 36.1° N)	TiO <sub>2</sub>	Rhodamine b, amoxicillin, <i>Escherichia coli</i>	2022	[7]
	0.077 m <sup>2</sup>	1 L	40 °C	23.6 W/m <sup>2</sup> (UV)	Japan (latitude: 36.1° N)	TiO <sub>2</sub>	<i>Chlorella vulgaris</i>	2023	[1]
FL	-	0.05 L	93 °C	15,000 W/m <sup>2</sup>	China (latitude: 34.5° N)	Cu-TiO <sub>2-x</sub>	Urea, urine	2022	[83]
V-groove	0.72 m <sup>2</sup>	10 L	-	-	Mexico (latitude: 19° N)	TiO <sub>2</sub>	Oxalic acid	2004	[79]
	0.057 m <sup>2</sup>	1 L	<38 °C	-	Spain (latitude: 37° N)	TiO <sub>2</sub>	<i>Escherichia coli</i>	2004	[80]
CPC	8.9 m <sup>2</sup>	247 L	-	-	Spain (latitude: 37.4° N)	TiO <sub>2</sub>	2,4-Dichlorophenol	1997	[76]
	4.5 m <sup>2</sup>	25 L	<40 °C	15–25 W/m <sup>2</sup> (UV)	Spain (latitude: 43° N)	TiO <sub>2</sub>	<i>Escherichia coli</i> , <i>Enterococcus faecalis</i>	1999	[84]
	3.08 m <sup>2</sup>	39 L	-	-	Morocco (latitude: 34° N)	TiO <sub>2</sub>	Azo-dyes	2002	[46]
	0.72 m <sup>2</sup>	10 L	-	-	Mexico (latitude: 19° N)	TiO <sub>2</sub>	Oxalic acid	2004	[79]
	0.057 m <sup>2</sup>	1 L	<38 °C	-	Spain (latitude: 37° N)	TiO <sub>2</sub>	<i>Escherichia coli</i>	2004	[80]
	3.08 m <sup>2</sup>	35 L	<45 °C	-	Spain (latitude: 37° N)	TiO <sub>2</sub>	Peptone, meat extract, urea, etc.	2004	[85]
	0.25 m <sup>2</sup>	11 L	15.8–36.5 °C	-	Spain (latitude: 37.4° N)	TiO <sub>2</sub>	<i>Escherichia coli</i>	2005	[86]
	3.08 m <sup>2</sup>	39 L	-	-	Spain (latitude: 37° N)	TiO <sub>2</sub>	Lincomycin	2005	[87]
	0.8 m <sup>2</sup>	17.5 L	25–48 °C	400 ± 25 W/m <sup>2</sup>	Spain (latitude: 40° N)	Ruthenium (II) tris-chelate complex	<i>Escherichia coli</i> , <i>Escherichia faecalis</i>	2006	[88]
0.4 m <sup>2</sup>	14 L	<30 °C	16.5 W/m <sup>2</sup> (UV)	Spain (latitude: 37.09° N)	TiO <sub>2</sub>	<i>Escherichia coli</i> , <i>Fusarium solani</i> , <i>Fusarium anthophilum</i>	2007	[89]	

Table 1. Cont.

Thematic Axis of Reactor	Dimension of Sunlight Reflector	Reactant Volume	Temperature	Irradiance	Deployed Location	Photocatalyst	Treatment Target	Timeline	Ref.
CPC	0.2 m <sup>2</sup>	7 L	<32 °C	2.8–7.2 W/m <sup>2</sup> (UV)	Spain (latitude: 37° N)	TiO <sub>2</sub>	<i>Escherichia coli</i>	2012	[90]
	0.25 m <sup>2</sup>	5–7 L	-	35–46 W/m <sup>2</sup> (UV)	Spain (latitude: 38.5° N)	TiO <sub>2</sub>	Acetaminophen, antipyrine, bisphenol A, caffeine, metoprolol and testosterone	2015	[91]
	Length: 1.2 m Width: 0.207 m	40 L	-	30 W/m <sup>2</sup> (UV)	Colombia (latitude: 3.5° N)	TiO <sub>2</sub>	17-β estradiol and noregestrol acetate	2015	[92]
		-	-	-	Colombia (latitude: 3.4° N)	TiO <sub>2</sub>		2017	[93]
	1 m <sup>2</sup>	20 L	26.1–38.2 °C	15.7–33.1 W/m <sup>2</sup> (UV)	Spain (latitude: 37.09° N)	TiO <sub>2</sub>	<i>Curvularia</i> sp.	2017	[94]
	0.228 m <sup>2</sup>	5 L	37 °C	-	Spain (latitude: 41.4° N)	TiO <sub>2</sub>	Valproic acid sodium salt	2017	[95]
	1 m <sup>2</sup>	15 L	16.6–43.2 °C	40 W/m <sup>2</sup> (UV)	Spain (latitude: 37.84° N)	TiO <sub>2</sub>	<i>Pseudomonas</i> , <i>Rheinheimera</i> and <i>Methylobacter</i>	2018	[96]
	0.228 m <sup>2</sup>	5 L	30 ± 5 °C	12.45–49.78 W/m <sup>2</sup> (UV)	Spain (latitude: 41.4° N)	TiO <sub>2</sub>	Diphenhydramine hydrochloride	2018	[97]
	-	100 L	-	-	Spain (latitude: 37.6° N)	TiO <sub>2</sub>	Endocrine disruptors	2018	[98]
	2.56 m <sup>2</sup>	11.4 L	-	≈2083 W/m <sup>2</sup>	China (latitude: 34.5° N)	Cd <sub>0.5</sub> Zn <sub>0.5</sub> S	Water splitting	2018	[48]
	1.74 m <sup>2</sup>	36 L	33 °C	1573 W/m <sup>2</sup>	Colombia (latitude: 10.2° N)	TiO <sub>2</sub>	Methylene blue, dichloroacetic acid, 4-Chlorophenol, phenol	2018	[73]
	1.74 m <sup>2</sup>	65 L		1259 W/m <sup>2</sup>					
	3.2 m <sup>2</sup>	35 L	-	30 W/m <sup>2</sup> (UV)	Spain (latitude: 37.09° N)	TiO <sub>2</sub> -rGO	Methomyl, Isoproturon, Alachlor	2020	[99]
	Width: 0.75 m Width: 3.6 m	-	-	-	U.S. (latitude: 38.5° N)	g-C <sub>3</sub> N <sub>4</sub> /chitosan	Atrazine, phenol, sulfamethoxazole, carbamazepine, <i>Escherichia coli</i>	2020	[100]
	1 m <sup>2</sup>	20 L	12–20 °C	664–1018 W/m <sup>2</sup>	Chile (latitude: 37.1° S)	Cu@C	Tartrazine	2022	[38]

#### 4.1. Solar Concentrated Type

##### 4.1.1. Parabolic Trough Reflector-Based Photoreactors

At present, solar-concentrated types of photoreactors mainly apply three technologies, including PTR, PDR and LFR. As a compact and efficient configuration for harvesting solar energy, it is not surprising that PTRs have been widely adopted as the basis for the construction of photocatalytic reactors [74–81,101]. As early as 1991, Anderson et al. reported a PTR-based photocatalytic reactor for groundwater remediation (shown in Figure 4a), which was widely considered to be the first on-site application project [101]. This project was built at the Lawrence Livermore Laboratory in the United States. The system structure consisted of rows of parabola troughs arranged in a field to form a trough array, which could reflect solar rays onto the reaction tube filled with photocatalyst particles. Subsequently, from 1993, a series of PTR-based photoreactors employing  $\text{TiO}_2$  as a photocatalyst for the degradation of various organic pollutants was tested and evaluated at the Plataforma Solar de Almeria (PSA), Spain. For example, Minero et al. established a large solar plant for the photocatalytic degradation of pentachlorophenol, which achieved a water treatment capacity of cubic meters per hour (Figure 4b) [78]. The system consisted of a total of twelve heliostat modules that could track solar motion, and every heliostat module was equipped with four PTRs. The nominal aperture area of each heliostat module was  $32 \text{ m}^2$ , thus providing sufficient light energy for the reaction tube. They also carried out the photocatalytic degradation of atrazine by employing one of the heliostat modules in the above solar plant, which exhibited an atrazine removal ratio of 98% in 2 h. Other photocatalytic experiments using PTR-based photoreactors include the inactivation of *Escherichia coli* [75], the elimination of methylene blue and rhodamine b [80] and the removal of oxalic acid [81]. In addition, experiments for the removal of harmful gases (such as toluene, acetaldehyde, etc.) were also carried out [74]. The above applications of PTRs in the design and development of photocatalytic reactors demonstrate their availability in photocatalysis. Moreover, it is worth noting that in addition to the combination of the heliostat and PTR configuration described above, PTR-based photoreactors can also be constructed by integrating an inclined plate with PTR. For instance, Barzegar et al. reported a parabolic solar collector unit [80] which comprised several PTR components located upon a  $30^\circ$  titled inclined plate (shown in Figure 4c). The system was established facing south to maximize the incident solar rays, and the reaction tubes in each PTR component were connected in sequence. Compared to the traditional heliostat–PTR configuration, since there is no need for a complex two-axis control mechanism, the PTR system equipped with an inclined plate could be more cost-effective, while a decrease in system efficiency might be inevitable.

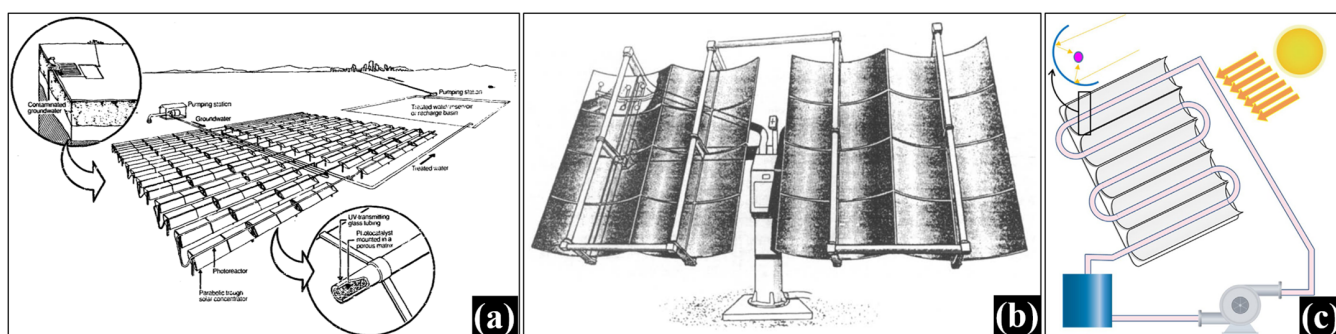


**Figure 4.** Configurations of parabolic trough collectors. (a) Parabolic trough-based photocatalytic system for treating contaminated groundwater (reused with permission from ref. [74]. Copyright 1991 Elsevier B.V.); (b) a heliostat-type parabolic trough-based photocatalytic system for degrading pentachlorophenol (reused with permission from ref. [75]. Copyright 1993 Elsevier B.V.); (c) a parabolic trough photoreactor installed on the inclined plate [81].

#### 4.1.2. Parabolic Dish Reflector-Based Photoreactors

Due to the high efficiency and compactness of PDR technology in concentrating solar energy, unique PDR-based photoreactors have also been explored. Oyama et al. presented a batch-mode photoreactor system aiming to achieve the photocatalytic degradation of commercial detergent under real sunlight (as shown in Figure 5) [82]. The system consisted of a round concave mirror (parabolic dish reflector) with an aperture diameter of 1.0 m and a flask-type reaction vessel. The parabolic dish reflector employed could achieve a geometric concentration ratio of 70 suns. The reaction vessel was mounted at the focal point of the parabolic dish for adsorbing the incident solar energy.  $\text{TiO}_2$ , as the photocatalyst, was used in suspension and flowed inside the system circulation loop. The photocatalytic degradation of the refractory detergent driven by concentrated sunlight exhibited a much higher treatment efficiency than conventional biodegradation.



**Figure 5.** Parabolic dish collector for photocatalytic degradation of detergent (adapted with permission from ref. [82]. Copyright 2004 Elsevier B.V.).

#### 4.1.3. Fresnel Condenser-Based Photoreactors

Linear Fresnel reflectors, due to their excellent solar energy harvesting capabilities and widely acknowledged low costs, have also shown strengths in the structural exploration of photocatalytic systems. Zhang et al. developed an LFR-based photoreactor for the photocatalytic treatment of various organic contaminants including organic dye, antibiotics and pathogenic microorganisms (Figure 6a) [7]. In this system, six flat primary mirrors were mounted on the pedestal of the reactor and driven by stepper motors. The system was located in the north–south direction, with the primary continuously tracking and reflecting solar rays to the reaction tubes. The quartz glass reaction tubes were located above the primary mirror array, which could be moved in a north–south direction to accommodate the solar altitude angle in different seasons. Different from previous studies employing  $\text{TiO}_2$  particles, this LFR-based photoreactor utilized  $\text{TiO}_2$ -coated silicone beads as the photocatalyst, which filled the inside of the reaction tubes. Rhodamine b, amoxicillin and *Escherichia coli* were successfully eliminated under actual weather conditions including a sunny day, cloudy day and rainy day, which demonstrated the feasibility of the LFR configuration for

providing solar energy to photocatalysis. In addition, Zhang et al. also reported the fabrication of an LFR-based microalgae biorefinery system [1]. Six flat mirrors were deployed as the primary mirror array for providing the solar flux to a transparent reaction box. The photocatalytic meshes, which were arranged in a stack, were installed inside the reaction box for receiving the reflected solar light. The microalgal solution could flow through the photocatalytic meshes and be destroyed by the photocatalytic effect, thereby achieving the release of carbohydrates, proteins and lipids. Moreover, Ma et al. carried out a hydrogen formation experiment through the photocatalytic conversion of aqueous urea and urine employing a Fresnel lens (FL) (shown in Figure 6b) [83], which provided ultra-high light irradiance ( $15,000 \text{ W/m}^2$ ) and a temperature close to the boiling point of water ( $93 \text{ }^\circ\text{C}$ ). A cascade reaction of heat-triggered urea hydrolysis and thermally assisted ammonia photolysis was established, which resulted in a high hydrogen formation efficiency.

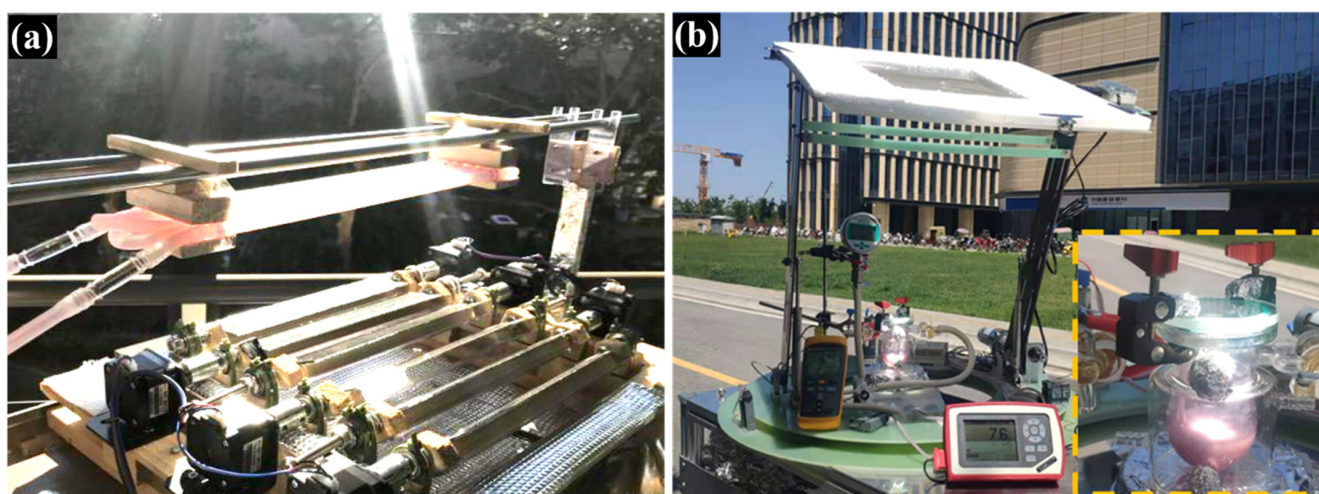


**Figure 6.** Fresnel condenser-based photoreactors. (a) A linear Fresnel collector for photocatalytic wastewater treatment (reused with permission from ref. [7]. Copyright 2023 Elsevier B.V.); (b) a Fresnel lens for photocatalytic conversion of aqueous urea and urine (adapted with permission from ref. [83]. Copyright 2022 Elsevier B.V.).

#### 4.1.4. Problems in Solar-Concentrated Photoreactors

Although solar energy-concentrated photocatalytic reactors have demonstrated the capability of improving photocatalytic efficiency, their inherent disadvantages appeared with further research. First, solar-concentrated photoreactors may provide excessively high light irradiance and reaction temperatures for photocatalytic reactions [17,102]. Figure 7a shows the ability of some typical PTRs [45,62,103–105], PDRs [49,106–108], SPTs [69] and LFRs [70,72,109] to concentrate solar energy. Usually, these solar concentrators are used to concentrate solar energy efficiently to produce high temperatures which can be employed in thermal engineering processes such as in photo-thermal power plants. A solar concentration ratio equivalent to hundreds or thousands of suns was achieved, resulting in ultra-high light irradiance (Figure 7a). For example, Mussard et al. reported a PTR system that could achieve a light irradiance of  $62,000 \text{ W/m}^2$  [104]. El Ouederni et al. carried out experimental tests and confirmed that the PDR could achieve a  $185,000 \text{ W/m}^2$  illumination irradiance [108]. In addition, Nepveu even used PDR to concentrate a light irradiance of  $1,068,000 \text{ W/m}^2$  [107]. LFR also achieved a light irradiance of more than  $17,000 \text{ W/m}^2$  [70]. Moreover, SPT has the capacity to achieve a light energy concentration of  $700,000 \text{ W/m}^2$  [69]. Due to a large amount of light energy converging, the photo-thermal conversion is also substantial, resulting in high temperatures.



Secondly, although PTR, PDR, SPT and LFR can achieve effective solar energy convergence under sunny conditions with sufficient direct light, their photothermal harvesting capability will plummet on cloudy days, thus greatly limiting the efficiency of the photocatalytic reaction [1,7]. Thirdly, for these solar concentrator configurations, complex mechanisms for driving these structures are unavoidable due to the need to actively track the incidence angle of the solar rays [17]. This would increase the overall design difficulty, construction investment, operation and maintenance costs of photocatalytic reactors. Due to the above issues, traditional CSP-based photoreactors, mainly PTRs, are widely considered to be an outdated technology. In order to find photoreactors that can achieve appropriate enhancement of natural solar energy for achieving promoted photocatalytic efficiency, non/low-concentrated photoreactors began to be developed.

#### 4.2. Non/Low-Concentrated Photoreactors

##### 4.2.1. V-Groove-Based Photoreactors

The V-groove, as a variant of the PTR, simplifies the profile of the parabola into two flat mirrors, thereby dramatically reducing the solar concentrating ratio (as shown in Figure 8a). V-groove-based photoreactors were mainly studied in 2004 by McLoughlin et al. and Bandala et al. to explore the advantages and disadvantages of PTR, V-groove and CPC technologies in photocatalytic applications [75,81].  $\text{TiO}_2$  was adopted as the photocatalyst for the degradation of various organic targets including oxalic acid and *Escherichia coli* under real sunlight. Due to the low concentration of sunlight, the reaction temperature of the V-groove-based photoreactor never exceeded  $38\text{ }^\circ\text{C}$ . In comparison experiments, the CPC-based photoreactor clearly demonstrated a higher photocatalytic efficiency compared to the V-groove-based photoreactor. This may be due to the fact that the V-groove has no optical focus; therefore, the flat mirror cannot effectively provide the reflected light to the reaction tube, thereby resulting in its low efficiency. As a transitional photocatalytic reactor technology, the V-groove-based photoreactor was quickly eliminated by CPC-based photoreactors.

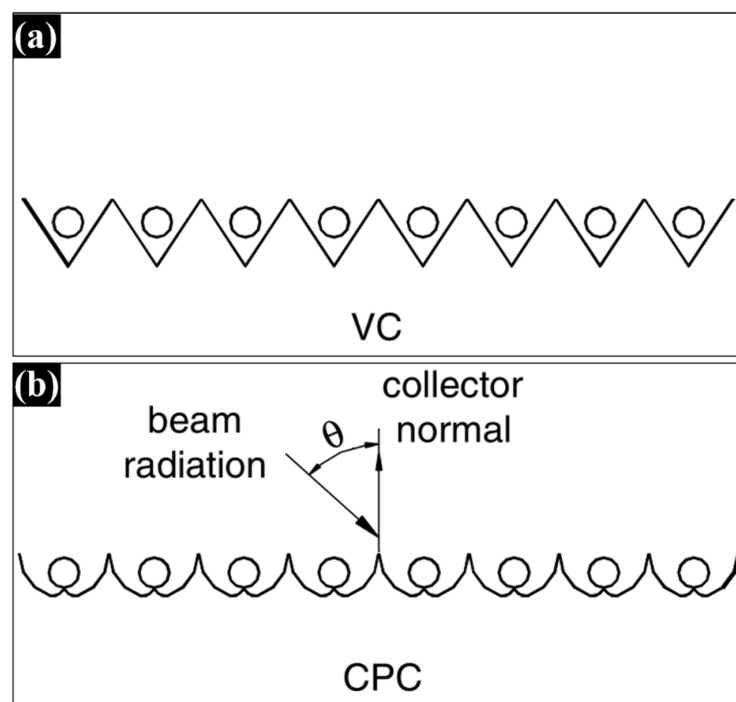


**Figure 8.** Cross sections of (a) V-groove and (b) compound parabolic collector-based photoreactors (adapted with permission from ref. [79]. Copyright 2004 Elsevier B.V.).

#### 4.2.2. Compound Parabolic Collector-Based Photoreactors

As mentioned above, in traditional applications, CPC was used as a secondary mirror for LFR, which has the unique advantage of being able to focus the light incoming from any direction to its focus point [17]. Applying a similar principle, under sunny conditions, a fixed CPC could focus direct solar light with different incidence angles at its focal point or reflect scattered light at its focal point on cloudy days. Due to the excellent adaptability of CPC to actual weather conditions, currently, CPC-based photoreactors (shown in Figure 8b) have gradually become the mainstream configuration of photocatalytic reactors, and a large number of CPC photoreactor experiments have been conducted (Table 1) [38,46,48,73,75,79,81,84–100]. For example, Malato et al. established a pilot-scaled CPC photoreactor for the degradation of 2,4-Dichlorophenol [79]. This system was inclined at  $37^\circ$  and located facing south. It was compared with a traditional PTR-based photoreactor under different weather conditions. Under sunny conditions, although the PTR provided much higher light irradiance (6–7 suns) than the CPC photoreactor (only 1 sun), no obvious difference was identified in their photocatalytic efficiencies. This study demonstrated that concentrating too much solar energy has limited value in improving photocatalytic efficiency. Meanwhile, under cloudy weather conditions, a significant improvement in the photocatalytic efficiency was achieved in the CPC photoreactor compared with the PTR photoreactor. This might be because, even in overcast conditions with scattered light, the CPC could still concentrate this light in different directions onto the reaction tube, whereas the PTR could not. This study clearly indicated the advantages of CPC over traditional PTR-based photoreactors, founding a new generation of photoreactors based on CPC technology.

Afterwards, another CPC-based treatment plant was established by Vidal et al. for detoxification and disinfection of contaminated water [84]. Various typical organic pollutants such as pesticides (EPTC, butiphos and  $\gamma$ -lindane) and microorganisms (*Escherichia coli*, *Enterococcus faecalis*) were selected as the treatment targets. All the organic contaminants were nearly 100% removed after 30 min of sunlight exposure, further demonstrating the applicability of CPC photoreactors to different treatment targets. Furthermore, a variant of CPC photoreactors has also been explored to promote its photocatalytic reaction performance. Ochoa-Gutiérrez et al. developed a new CPC photoreactor prototype (named OMTP), adopting multiple reaction tubes for the degradation of several water contaminants (methylene blue, dichloroacetic acid, 4-chlorophenol and phenol) [73]. Compared to a traditional CPC photoreactor, which was installed with only one reaction tube, the OMTP demonstrated its improved photocatalytic treatment efficiency across all of the selected contaminants. This was due to the much-enhanced ratio of the solar irradiated area to the reactant volume in the OMTP, which benefited from the boosted activation of photocatalysts, thereby leading to a superior efficiency. The above early studies of CPC photoreactors have preliminarily confirmed their applicability in photocatalysis, especially highlighting their excellent adaptability to real weather.

In recent years, to further enhance the efficiency of CPC photoreactors in different application directions, photocatalysts with improved solar response capabilities were applied. Luna-Sanguino et al. investigated the degradation of harmful pesticides (methomyl, isoproturon and alachlor) by a CPC photoreactor [99]. In this study, a composite photocatalyst combining  $\text{TiO}_2$  with reduced graphene oxide ( $\text{TiO}_2$ -rGO) was utilized, which possessed broader absorption in the solar visible spectrum region compared with  $\text{TiO}_2$  alone. Cao et al. reported several CPC-based water splitting photoreactor systems employing a composite photocatalyst ( $\text{Cd}_{0.5}\text{Zn}_{0.5}\text{S}$ ) and sacrificial agent ( $\text{Na}_2\text{S}/\text{Na}_2\text{SO}_3$ ) [48]. Their CPC system was developed over three generations. The first generation was installed in a closed indoor condition, which utilized the Xe lamp as a light source. Then, a lab-scaled CPC hydrogen production unit was deployed under real sunlight conditions, which was reported to be the first reactor to achieve direct solar photocatalytic hydrogen production. A third-generation CPC photoreactor built to a pilot scale was also deployed under real sunlight, while the reaction medium was naturally circulated to reduce the overall operating energy consump-

tion. Moreover, Muñoz-Flores et al. reported a pilot-scale CPC photoreactor adopting a carbon-containing Cu-based (Cu@C) photocatalyst for the degradation of tartrazine [38]. Compared to the traditional TiO<sub>2</sub>, which has low photoactivity under visible light, the employed Cu@C, as a visible light-responsive composite photocatalyst, could be excited not only by UV, but also by the solar visible light, containing significant energy. Therefore, this CPC photoreactor showed a high photocatalytic efficiency.

Despite the above encouraging application of CPC photoreactors in photocatalysis and the continued efficiency improvements brought by numerous efforts, some shortcomings specific to the CPC structure still need to be noted. First of all, although CPC could facilitate light converge uniformly on the reaction tube to a certain extent, it would inevitably cause excessive light irradiance and overheating in some areas of the reaction tube [73]. Therefore, in order to achieve the ideal uniform distribution of light energy on the reaction tube, intensive optimization work and fine assembly of the CPC components are required. On the other hand, manufacturing CPC mirrors, as precision optical devices, poses an additional challenge beyond their complex design and optimization. Ensuring the mirror is produced according to the design blueprint may be also a challenge that needs to be faced. Additionally, the CPC mirrors used in actual engineering are usually manufactured through high-temperature hot bending processes; therefore, this relatively high-cost reflector may also raise some concerns for large-scale application of CPC photoreactors.

## 5. Relevant Problems in CSP-Based Photoreactors

Due to the variability of actual weather and the complexity of real industrial processes, CSP technology-based photoreactors may also face multiple challenges in the future real large-scale application scenarios. The following sections envisage some of the issues of interest, addressing which may advance the application of CSP technology in photocatalysis and ultimately contribute to the sustainable development of society.

### 5.1. Instability of Real Weather

Although solar energy is an ideal energy source that is widely distributed and could be utilized at a low cost, the actual weather inevitably causes instability in the natural solar energy reaching the ground [7]. For the photocatalytic process, appropriate light irradiance is required to maximize the excitation of the photocatalyst and favorable heat energy is required to promote the reaction rate [7]. Therefore, natural variations in solar energy could inevitably affect the photocatalytic reaction rate. It also needs to be pointed out that modern industrial processes pursue the high robustness of system operation, and uncontrolled decline in the production rate is usually unacceptable. Therefore, if solar-energy-driven photocatalysis technology is to be truly extended to large-scale industrial processes (such as wastewater treatment, hydrogen production, biomass conversion, etc.), searching for solutions that could mitigate or even avoid the effects of natural solar variability on photocatalytic rates needs to be prioritized.

At present, some efforts have been put into solving this problem by researchers. In the development of a photocatalytic reactor based on a linear Fresnel concentrator constructed by Zhang et al., a novel solar energy regulation strategy was employed [7]. Traditional linear Fresnel concentrators utilize multiple primary mirrors to track the sun's movement and reflect the sunlight to the focus to obtain ultra-high energy. Meanwhile, in their reactors, the innovation is that each primary mirror was controlled to rotate through its own independent control system. Under different weather conditions and at different times during the day, there were different numbers of primary mirrors used to focus sunlight. On sunny days when natural sunlight is strong, only two or three primary mirrors focus sunlight on the photocatalytic reaction tube, thus providing superior light irradiance and reaction temperatures for maximizing photocatalytic efficiency. Meanwhile, under cloudy, overcast and other weather conditions with weak natural sunlight, all the primary mirrors participate in the convergence of solar energy to provide optimized light irradiance and reaction temperatures to the photocatalytic reaction. Compared with the

reactor that passively receives solar energy, the photocatalytic reaction rate of this solar concentration-controlled reactor was increased by more than 200% [7], thus demonstrating the great potential of this solar control strategy in photocatalytic applications. A similar solar optimization control system has also been successfully adopted by Zhang et al. in another reactor for microalgae biorefining, further demonstrating the broad applicability of this strategy [1]. The above studies provided empirical experience for realizing efficient and stable photocatalytic reactions driven by real sunlight and promoted the practical process of photocatalytic technology. However, for other CSP configurations such as PTR, SPT and PDR, how to realize the effective regulation and optimization of solar energy is still a topic worth exploring.

### 5.2. Nighttime Operation

Photocatalytic reactions require continuous input of light and heat energy to proceed smoothly. Considering the requirement of high robustness for actual industrial process, it is also a challenge to maintain efficient photocatalytic processes at night when there is no natural sunlight. The adoption of artificial light sources for nighttime photocatalytic lighting is straightforward in theory, but in the actual engineering project design, it is necessary to integrate the natural sunlight collector with the artificial light source. Portela et al. proposed a new solar/lamp-irradiated CPC photoreactor for air treatment [9]. The designed tubular photoreactor consisted of two concentric borosilicate glass tubes, and the space between them was filled with a photocatalyst. Natural solar light was employed as the radiation energy source under sunny conditions during the daytime, which was reflected onto the reaction tube. While during the nighttime and totally overcast conditions, since there was almost no natural light source, an artificial lamp was used as the complement of natural solar energy to activate the photocatalyst, thus allowing 24 h operation in any climate. An automated system was used to switch on or off the lamp depending on the natural light radiation. In the photocatalytic conversion of  $H_2S$ , this system demonstrated a sustained reaction capability, demonstrating its availability under real solar conditions. This study provided an idea of a compact reactor layout for designing photocatalytic reactions that could continuously carry out 24 h operation.

### 5.3. Configuration of Photocatalyst Immobilization Substrate

Most CSP-based photoreactors utilize suspended photocatalysts, which may lead to complex post-separation and increased operating costs. In order to facilitate the large-scale application of photocatalytic technology, the immobilized photocatalyst needs to be equipped in the photoreactors.

In the previous studies, Villén et al. tested the efficiency of two CPC prototypes with different substrate configurations of photocatalysts, namely coaxial- and a fin-type photocatalysts (as shown in Figure 9a) [88]. The results demonstrated that the fin-type photochemical reactor always showed higher inactivation of waterborne bacteria than the coaxial-type reactor. This phenomenon might be due to the lower moving rate of water flowing through the fin-type system, which may lead to a higher number of bacteria attached to the immobilized photocatalyst. Additionally, Alrousan et al. studied the photocatalytic disinfection efficiency in CPC photoreactors equipped with several kinds of photocatalyst-immobilized configurations (as shown in Figure 9b) [90]. The substrate structures included an uncoated single tube, coated single tube, coated double coaxial tube, coated external–uncoated internal coaxial tube, uncoated external–coated internal coaxial tube and uncoated double coaxial tube. Compared with the coated external–uncoated internal coaxial tube system, the uncoated external–coated internal coaxial tube exhibited a significant enhancement in its sterilization capability, which may be because the latter configuration could make use of all the available incident UV solar energy for photolytic inactivation. Meanwhile, the concentric coated tube arrangement showed the highest efficiency among these supporting structures owing to its superior light utilization capability. More recently, Zhang et al. integrated stacked photocatalytic meshes with an

LFR photoreactor [1]. These photocatalytic meshes were inclined at  $36.1^\circ$  to receive real solar energy vertically, thus ensuring the maximized acceptance of incident solar energy. Additionally, a spacing interval of 2 mm was kept between adjacent mesh, thereby not only allowing the reactant to flow smoothly, but also improving the mass transfer rate during the reaction. Moreover, all the photocatalytic meshes were arranged into a three-layer stacked configuration, which not only ensured the maximum utilization of light energy but also reduced the complexity of the system design.

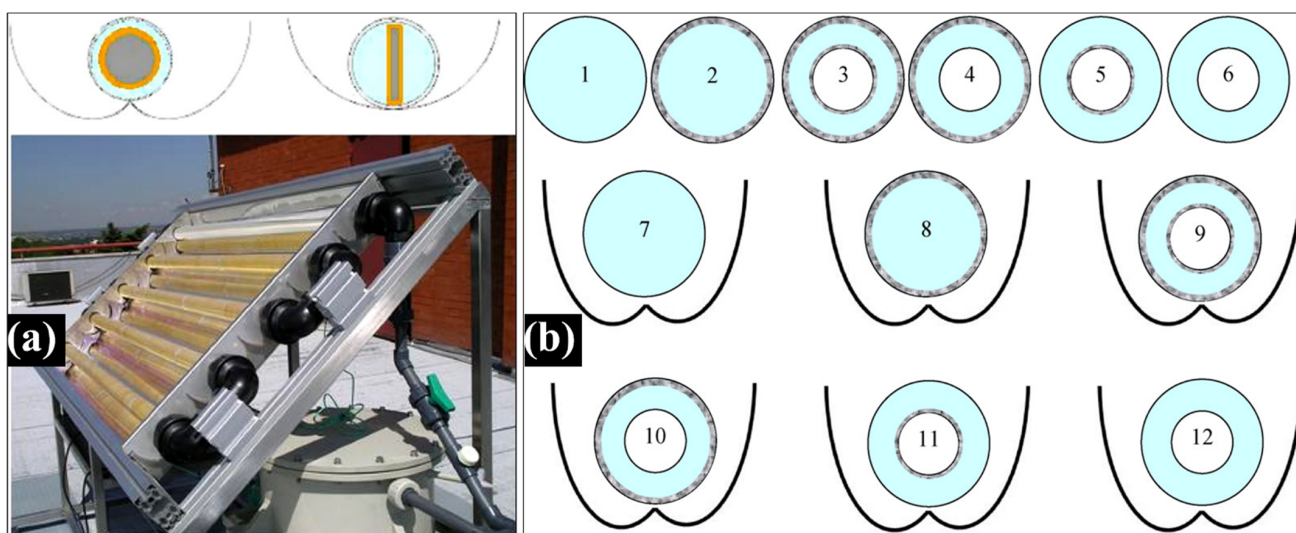


**Figure 9.** Configurations of photocatalyst immobilization substrates. (a) Comparison of coaxial-type and fin-type CPC photoreactors (reused with permission from ref. [88]. Copyright 2006 Elsevier B.V.); (b) CPC photoreactor equipped with several photocatalyst-immobilized configurations (reused with permission from ref. [90]. Copyright 2012 Elsevier B.V.).

It is worth noting that the above-mentioned development and optimization of the supporting configuration of the immobilized photocatalysts are all oriented towards specific application scenarios (e.g., sterilization and microalgae processing). The conclusions obtained may not be applicable to a wide range of application scenarios. For other application scenarios (such as gas-phase treatment, water treatment, water splitting, etc.) and different working conditions (such as reactant concentrations, flow rates, etc.), appropriate catalyst substrate configurations are needed. Generally, in a CSP-based photoreactor, the immobilization of photocatalyst may need to meet the following requirements: (1) achieve effective incident light energy utilization; (2) avoid obstructing the flow of the reactant and (3) load a large amount of photocatalyst. Based on the above requirements, an immobilization substrate and configuration that are suitable for CSP-based photocatalytic reactors need to be designed correspondingly.

#### 5.4. Economic Analysis

An economic evaluation is one of the criteria used to judge whether a new technology can be applied to practical applications. Due to the absence of practical application examples of large-scale photocatalytic facilities, an economic analysis of photocatalytic reactors is required. In a study by Vidal et al., a large-scale CPC photocatalytic wastewater treatment plant with an occupied area of  $500 \text{ m}^2$  was assumed [84]. The operation cost of this plant was estimated to be 0.7 USD for  $1 \text{ m}^3$  water treatment (based on 1997 construction cost indices), which exhibited excellent cost-effectiveness compared with conventional technologies (around 1.0 dollars/ $\text{m}^3$ ). Then, Vela et al. carried out an economic comparison of CPC photoreactors using different photocatalysts ( $\text{ZnO}$  and  $\text{TiO}_2$ ) [98]. Assuming 365 sunny days in a year and 8 h of system operation per day, the cost per cubic meter of water treated by the  $\text{TiO}_2$ -adopted CPC photoreactor was 1.45-fold higher than that of the  $\text{ZnO}$

system. The difference in process cost caused by the different catalysts was mainly due to the different times the catalysts required for pollutants degradation. Additionally, it was also found that different weather had a significant impact on the system operating cost. The cost of photocatalytic wastewater treatment under real whole-year weather condition was estimated to be 1.40-fold higher than that of ideal year-round sunny conditions, which was due to the inefficient photocatalytic rate on cloudy days. These results further indicated that the stable operation of a CSP-based photoreactor under different weather conditions might be an urgent problem to be solved, as mentioned in Section 5.1. Furthermore, Zhang et al. also implemented a global economic analysis of a LFR photoreactor, which indicated that photocatalytic reactors have significant application potential in every country [1]. However, due to latitude, altitude, climate and other actual factors, the performance of photocatalytic reactors in different countries would be significantly different, and generally, photocatalytic reactors deployed in low-latitude countries could be more effective than in high-latitude countries. Despite studies evaluating photocatalytic reactors from different perspectives that have been proposed, a more comprehensive and professional evaluation of the establishment of real large-scale plants needs to be conducted rigorously.

## 6. Prospects for Further Work

At present, photocatalytic reactors developed based on CSP technology have shown encouraging application potential in photocatalytic water purification and energy conversion, which has laid the foundation for the early realization of sustainable social development. However, most of the developed CSP-based photoreactors are still in the batch stage, lacking application capabilities in real situations. For industrial and large-scale application scenarios, the establishment of a flow reactor system is necessary, while it requires further technological maturity to promote the realization of this goal. In the past 5 years, some important research results have been obtained, which may set future trends for the future development of CSP-based photoreactors. For example, the solar energy controllable strategy proposed in 2021 could provide optimized light irradiance and temperature for photocatalytic reactions under unstable real solar conditions [7], which provides a reference for the design of efficient and stable photocatalytic reactors in the future. In addition, the installation of multiple reaction tubes in a photoreactor reported in 2018 could improve the ratio of solar irradiated area to reactant volume, which provides a new way for further improving the reaction efficiency [73]. Additionally, the multilayer stacked photocatalytic mesh system proposed in 2023 could achieve efficient reception of solar energy, a large amount of photocatalyst loading, smooth flow of reactants and long-term stability, providing a feasible technical solution to solve the problem of post-separation [1]. The economic evaluation conducted in 2018 clearly indicated that the use of high-performance catalysts in CSP-based photoreactors could significantly reduce reactor operating costs [98]. Visible light-activated photocatalysts, such as graphene oxide-modified  $\text{Ag}/\text{Ag}_2\text{O}/\text{BiPO}_4/\text{Bi}_2\text{WO}_6$  developed in 2022 [20], showed excellent photocatalytic capabilities for the removal of organic pollutants and bacteria, sharing great potential to be utilized in future CSP-based photoreactors. Based on the above recent studies, future development of CSP-based photoreactors may focus on the innovation in the reactor structure and the application of high-performance immobilized photocatalysts. These advancements will facilitate the achievement of high-efficiency photocatalytic reactions and low system costs, finally realizing industrial applications.

## 7. Conclusions

This review illustrated the application of CSP technology in photocatalysis based on three dimensions: the development history of photoreactors, current technical challenges and future work. Efficient photocatalytic reactions require appropriate light irradiance and temperatures, and the low energy density of natural solar energy highlights the necessity of combining CSP technology with photocatalysis. Although existing CSP-based photoreactor technology has significantly improved the practical availability of photocatalysis, the challenges in unstable real weather, nighttime operation, post-separation and economic

concern remain to be solved. Based on the latest reports, the adoption of a solar energy control strategy, employment of UV-visible responsive photocatalyst and immobilization substrate, innovations in reactor structure, economic evaluation of systems and establishment of reactor industry standards may be favorable for technological breakthroughs and engineering applications of future CSP-based photoreactors.

**Author Contributions:** Conceptualization, C.Z.; methodology, C.Z.; software, C.Z.; validation, C.Z.; formal analysis, C.Z. and N.L.; investigation, C.Z.; resources, G.A.; data curation, C.Z.; writing—original draft preparation, C.Z.; writing—review and editing, C.Z., G.A. and N.L.; visualization, C.Z.; supervision, G.A.; project administration, N.L. and G.A.; funding acquisition, C.Z. All authors have read and agreed to the published version of the manuscript.

**Funding:** This research was funded by the Science and Technology Innovation Project 2021 under grant number XHD2021-002 and the Science and Technology Innovation Project 2022 under grant number XHD2022-003 from the Foshan Xianhu Laboratory.

**Conflicts of Interest:** The authors declare no conflicts of interest.

## References

1. Zhang, C.; Ming, J.; Sun, X.; Zhu, Y.; An, G.; Chen, G.; Yang, Y. Development of a Green and Efficient Photocatalytic Mesh Microalgae Biorefinery (PMMB) System for Sustainable Biomass Conversion under Real Solar Light. *Chem. Eng. J.* **2023**, *466*, 143260. [[CrossRef](#)]
2. Akpan, J.O.O. Sustainable Energy Development: History and Recent Advances. *Energies* **2023**, *16*, 7049. [[CrossRef](#)]
3. Ming, J.; Sun, X.; Ma, Q.; Liu, N.; Zhang, C.; Kawazoe, N.; Chen, G.; Yang, Y. Advanced Photocatalytic Sterilization for Recalcitrant Enterococcus Sp. Contaminated Water by Newly Developed Z-Scheme Bi<sub>2</sub>WO<sub>6</sub> Based Composites under Solar Light. *Chemosphere* **2023**, *310*, 136912. [[CrossRef](#)] [[PubMed](#)]
4. Ma, Q.; Hu, X.; Liu, N.; Sharma, A.; Zhang, C.; Kawazoe, N.; Chen, G.; Yang, Y. Polyethylene Glycol (PEG)-Modified Ag/Ag<sub>2</sub>O/Ag<sub>3</sub>PO<sub>4</sub>/Bi<sub>2</sub>WO<sub>6</sub> Photocatalyst Film with Enhanced Efficiency and Stability under Solar Light. *J. Colloid Interface Sci.* **2020**, *569*, 101–113. [[CrossRef](#)] [[PubMed](#)]
5. Zhu, Q.; Liu, N.; Ma, Q.; Sharma, A.; Nagai, D.; Sun, X.; Zhang, C.; Yang, Y. Sol-Gel/Hydrothermal Two-Step Synthesis Strategy for Promoting Ag Species-Modified TiO<sub>2</sub>-Based Composite Activity toward H<sub>2</sub> Evolution under Solar Light. *Mater. Today Energy* **2021**, *20*, 100648. [[CrossRef](#)]
6. Hu, X.; Ma, Q.; Wang, X.; Yang, Y.; Liu, N.; Zhang, C.; Kawazoe, N.; Chen, G.; Yang, Y. Layered Ag/Ag<sub>2</sub>O/BiPO<sub>4</sub>/Bi<sub>2</sub>WO<sub>6</sub> Heterostructures by Two-Step Method for Enhanced Photocatalysis. *J. Catal.* **2020**, *387*, 28–38. [[CrossRef](#)]
7. Zhang, C.; Liu, N.; Ming, J.; Sharma, A.; Ma, Q.; Liu, Z.; Chen, G.; Yang, Y. Development of a Novel Solar Energy Controllable Linear Fresnel Photoreactor (LFP) for High-Efficiency Photocatalytic Wastewater Treatment under Actual Weather. *Water Res.* **2022**, *208*, 117880. [[CrossRef](#)]
8. Bi, Y.; Ouyang, S.; Umezawa, N.; Cao, J.; Ye, J. Facet Effect of Single-Crystalline Ag<sub>3</sub>PO<sub>4</sub> Sub-Microcrystals on Photocatalytic Properties. *J. Am. Chem. Soc.* **2011**, *4*, 6490–6492. [[CrossRef](#)]
9. Portela, R.; Suárez, S.; Tessinari, R.F.; Hernández-Alonso, M.D.; Canela, M.C.; Sánchez, B. Solar/Lamp-Irradiated Tubular Photoreactor for Air Treatment with Transparent Supported Photocatalysts. *Appl. Catal. B Environ.* **2011**, *105*, 95–102. [[CrossRef](#)]
10. Liu, N.; Zhu, Q.; Zhang, N.; Zhang, C.; Kawazoe, N.; Chen, G.; Negishi, N.; Yang, Y. Superior Disinfection Effect of Escherichia Coli by Hydrothermal Synthesized TiO<sub>2</sub>-Based Composite Photocatalyst under LED Irradiation: Influence of Environmental Factors and Disinfection Mechanism. *Environ. Pollut.* **2019**, *247*, 847–856. [[CrossRef](#)] [[PubMed](#)]
11. Zhang, G.; Lan, Z.A.; Lin, L.; Lin, S.; Wang, X. Overall Water Splitting by Pt/g-C<sub>3</sub>N<sub>4</sub> Photocatalysts without Using Sacrificial Agents. *Chem. Sci.* **2016**, *7*, 3062–3066. [[CrossRef](#)]
12. Liu, J.; Liu, Y.; Liu, N.; Han, Y.; Zhang, X.; Huang, H.; Lifshitz, Y.; Lee, S.T.; Zhong, J.; Kang, Z. Metal-Free Efficient Photocatalyst for Stable Visible Water Splitting via a Two-Electron Pathway. *Science* **2015**, *347*, 970–974. [[CrossRef](#)]
13. Reli, M.; Edelmannová, M.; Šihor, M.; Praus, P.; Svoboda, L.; Mamulová, K.K.; Otoupalíková, H.; Čapek, L.; Hospodková, A.; Obalová, L.; et al. Photocatalytic H<sub>2</sub> Generation from Aqueous Ammonia Solution Using ZnO Photocatalysts Prepared by Different Methods. *Int. J. Hydrogen Energy* **2015**, *40*, 8530–8538. [[CrossRef](#)]
14. Kominami, H.; Nishimune, H.; Ohta, Y.; Arakawa, Y.; Inaba, T. Photocatalytic Hydrogen Formation from Ammonia and Methyl Amine in an Aqueous Suspension of Metal-Loaded Titanium(IV) Oxide Particles. *Appl. Catal. B Environ.* **2012**, *111–112*, 297–302. [[CrossRef](#)]
15. Vidyasagar, D.; Ghugal, S.G.; Kulkarni, A.; Mishra, P.; Shende, A.G.; Jagannath; Umare, S.S.; Sasikala, R. Silver/Silver(II) Oxide (Ag/AgO) Loaded Graphitic Carbon Nitride Microspheres: An Effective Visible Light Active Photocatalyst for Degradation of Acidic Dyes and Bacterial Inactivation. *Appl. Catal. B Environ.* **2018**, *221*, 339–348. [[CrossRef](#)]
16. Deng, J.; Liang, J.; Li, M.; Tong, M. Enhanced Visible-Light-Driven Photocatalytic Bacteria Disinfection by g-C<sub>3</sub>N<sub>4</sub>-AgBr. *Colloids Surf. B Biointerfaces* **2017**, *152*, 49–57. [[CrossRef](#)]

17. Braham, R.J.; Harris, A.T. Review of Major Design and Scale-up Considerations for Solar Photocatalytic Reactors. *Ind. Eng. Chem. Res.* **2009**, *48*, 8890–8905. [[CrossRef](#)]
18. Ajbar, W.; Hernández, J.A.; Parrales, A.; Torres, L. Thermal Efficiency Improvement of Parabolic Trough Solar Collector Using Different Kinds of Hybrid Nanofluids. *Case Stud. Therm. Eng.* **2023**, *42*, 102759. [[CrossRef](#)]
19. Desai, N.B.; Bandyopadhyay, S. Optimization of Concentrating Solar Thermal Power Plant Based on Parabolic Trough Collector. *J. Clean. Prod.* **2015**, *89*, 262–271. [[CrossRef](#)]
20. Ma, Q.; Ming, J.; Sun, X.; Liu, N.; Chen, G.; Yang, Y. Visible Light Active Graphene Oxide Modified Ag/Ag<sub>2</sub>O/BiPO<sub>4</sub>/Bi<sub>2</sub>WO<sub>6</sub> for Photocatalytic Removal of Organic Pollutants and Bacteria in Wastewater. *Chemosphere* **2022**, *306*, 135512. [[CrossRef](#)]
21. Jafarova, V.N.; Orudzhev, G.S. Structural and Electronic Properties of ZnO: A First-Principles Density-Functional Theory Study within LDA(GGA) and LDA(GGA)+U Methods. *Solid State Commun.* **2021**, *325*, 114166. [[CrossRef](#)]
22. Huang, C.K.; Wu, T.; Huang, C.W.; Lai, C.Y.; Wu, M.Y.; Lin, Y.W. Enhanced Photocatalytic Performance of BiVO<sub>4</sub> in Aqueous AgNO<sub>3</sub> Solution under Visible Light Irradiation. *Appl. Surf. Sci.* **2017**, *399*, 10–19. [[CrossRef](#)]
23. Lee, S.S.; Bai, H.; Liu, Z.; Sun, D.D. Electrospun TiO<sub>2</sub>/SnO<sub>2</sub> Nanofibers with Innovative Structure and Chemical Properties for Highly Efficient Photocatalytic H<sub>2</sub> Generation. *Int. J. Hydrogen Energy* **2012**, *37*, 10575–10584. [[CrossRef](#)]
24. Yao, W.; Song, X.; Huang, C.; Xu, Q.; Wu, Q. Enhancing Solar Hydrogen Production via Modified Photochemical Treatment of Pt/CdS Photocatalyst. *Catal. Today* **2013**, *199*, 42–47. [[CrossRef](#)]
25. Zeng, P.; Zhang, Q.; Zhang, X.; Peng, T. Graphite Oxide-TiO<sub>2</sub> Nanocomposite and Its Efficient Visible-Light-Driven Photocatalytic Hydrogen Production. *J. Alloys Compd.* **2012**, *516*, 85–90. [[CrossRef](#)]
26. Kim, J.; Kang, M. High Photocatalytic Hydrogen Production over the Band Gap-Tuned Urchin-like Bi<sub>2</sub>S<sub>3</sub>-Loaded TiO<sub>2</sub> Composites System. *Int. J. Hydrogen Energy* **2012**, *37*, 8249–8256. [[CrossRef](#)]
27. Liu, J.; Cheng, B.; Yu, J. A New Understanding of the Photocatalytic Mechanism of the Direct Z-Scheme g-C<sub>3</sub>N<sub>4</sub>/TiO<sub>2</sub> Heterostructure. *Phys. Chem. Chem. Phys.* **2016**, *18*, 31175–31183. [[CrossRef](#)]
28. Wunderlich, W.; Oekermann, T.; Miao, L.; Hue, N.T.; Tanemura, S.; Tanemura, M. Electronic Properties of Nano-Porous TiO<sub>2</sub>- and ZnO-Thin Films-Comparison of Simulations and Experiments. *J. Ceram. Process. Res.* **2004**, *5*, 343–354.
29. Lei, Z.; You, W.; Liu, M.; Zhou, G.; Takata, T.; Hara, M.; Domen, K.; Li, C. Photocatalytic Water Reduction under Visible Light on a Novel ZnIn<sub>2</sub>S<sub>4</sub> Catalyst Synthesized by Hydrothermal Method. *Chem. Commun.* **2003**, *3*, 2142–2143. [[CrossRef](#)]
30. Wang, X.; Li, S.; Yu, H.; Yu, J.; Liu, S. Ag<sub>2</sub>O as a New Visible-Light Photocatalyst: Self-Stability and High Photocatalytic Activity. *Chem. A Eur. J.* **2011**, *17*, 7777–7780. [[CrossRef](#)] [[PubMed](#)]
31. Hu, X.; Zhu, Q.; Wang, X.; Kawazoe, N.; Yang, Y. Nonmetal-Metal-Semiconductor-Promoted P/Ag/Ag<sub>2</sub>O/Ag<sub>3</sub>PO<sub>4</sub>/TiO<sub>2</sub> Photocatalyst with Superior Photocatalytic Activity and Stability. *J. Mater. Chem. A* **2015**, *3*, 17858–17865. [[CrossRef](#)]
32. Maeda, K.; Lu, D.; Domen, K. Direct Water Splitting into Hydrogen and Oxygen under Visible Light by Using Modified Taon Photocatalysts with D0 Electronic Configuration. *Chem. A Eur. J.* **2013**, *19*, 4986–4991. [[CrossRef](#)]
33. Kim, H.G.; Hwang, D.W.; Kim, J.; Kim, Y.G.; Lee, J.S. Highly Donor-Doped (110) Layered Perovskite Materials as Novel Photocatalysts for Overall Water Splitting. *Chem. Commun.* **1999**, *2*, 1077–1078. [[CrossRef](#)]
34. Dhanasekaran, P.; Gupta, N.M. Factors Affecting the Production of H<sub>2</sub> by Water Splitting over a Novel Visible-Light-Driven Photocatalyst GaFeO<sub>3</sub>. *Int. J. Hydrogen Energy* **2012**, *37*, 4897–4907. [[CrossRef](#)]
35. Wang, Y.; Ge, H.X.; Chen, Y.P.; Meng, X.Y.; Ghanbaja, J.; Horwat, D.; Pierson, J.F. Wurtzite CoO: A Direct Band Gap Oxide Suitable for a Photovoltaic Absorber. *Chem. Commun.* **2018**, *54*, 13949–13952. [[CrossRef](#)]
36. Hu, S.P.; Xu, C.Y.; Zhen, L. Solvothermal Synthesis of Bi<sub>2</sub>WO<sub>6</sub> Hollow Structures with Excellent Visible-Light Photocatalytic Properties. *Mater. Lett.* **2013**, *95*, 117–120. [[CrossRef](#)]
37. Basu, M.; Sinha, A.K.; Pradhan, M.; Sarkar, S.; Negishi, Y.; Govind; Pal, T. Evolution of Hierarchical Hexagonal Stacked Plates of CuS from Liquid–Liquid Interface and Its Photocatalytic Application for Oxidative Degradation of Different Dyes under Indoor Lighting. *Environ. Sci. Technol.* **2010**, *44*, 6313–6318. [[CrossRef](#)] [[PubMed](#)]
38. Muñoz-Flores, P.; Poon, P.S.; Ania, C.O.; Matos, J. Performance of a C-Containing Cu-Based Photocatalyst for the Degradation of Tartrazine: Comparison of Performance in a Slurry and CPC Photoreactor under Artificial and Natural Solar Light. *J. Colloid Interface Sci.* **2022**, *623*, 646–659. [[CrossRef](#)]
39. Reutergrårdh, L.B.; Iangphasuk, M. Photocatalytic Decolourization of Reactive Azo Dye: A Comparison between TiO<sub>2</sub> and CdS Photocatalysis. *Chemosphere* **1997**, *35*, 585–596. [[CrossRef](#)]
40. Askari, N.; Beheshti, M.; Mowla, D.; Farhadian, M. Facile Construction of Novel Z-Scheme MnWO<sub>4</sub>/Bi<sub>2</sub>S<sub>3</sub> Heterojunction with Enhanced Photocatalytic Degradation of Antibiotics. *Mater. Sci. Semicond. Process.* **2021**, *127*, 105723. [[CrossRef](#)]
41. Yu, J.; Kiwi, J.; Zivkovic, I.; Rønnow, H.M.; Wang, T.; Rtimi, S. Quantification of the Local Magnetized Nanotube Domains Accelerating the Photocatalytic Removal of the Emerging Pollutant Tetracycline. *Appl. Catal. B Environ.* **2019**, *248*, 450–458. [[CrossRef](#)]
42. Castro-Alfárez, M.; Polo-López, M.I.; Marugán, J.; Fernández-Ibáñez, P. Mechanistic Model of the Escherichia Coli Inactivation by Solar Disinfection Based on the Photo-Generation of Internal ROS and the Photo-Inactivation of Enzymes: CAT and SOD. *Chem. Eng. J.* **2017**, *318*, 214–223. [[CrossRef](#)]
43. Chen, Y.; Wang, Y.; Li, W.; Yang, Q.; Hou, Q.; Wei, L.; Liu, L.; Huang, F.; Ju, M. Enhancement of Photocatalytic Performance with the Use of Noble-Metal-Decorated TiO<sub>2</sub> Nanocrystals as Highly Active Catalysts for Aerobic Oxidation under Visible-Light Irradiation. *Appl. Catal. B Environ.* **2017**, *210*, 352–367. [[CrossRef](#)]

44. Abbas, M.; Boumeddane, B.; Said, N.; Chikouche, A. Dish Stirling Technology: A 100 MW Solar Power Plant Using Hydrogen for Algeria. *Int. J. Hydrogen Energy* **2011**, *36*, 4305–4314. [[CrossRef](#)]
45. Balghouthi, M.; Chahbani, M.H.; Guizani, A. Investigation of a Solar Cooling Installation in Tunisia. *Appl. Energy* **2012**, *98*, 138–148. [[CrossRef](#)]
46. Augugliaro, V.; Baiocchi, C.; Prevot, A.B.; García-López, E.; Loddo, V.; Malato, S.; Marci, G.; Palmisano, L.; Pazzi, M.; Pramauro, E. Azo-Dyes Photocatalytic Degradation in Aqueous Suspension of TiO<sub>2</sub> under Solar Irradiation. *Chemosphere* **2002**, *49*, 1223–1230. [[CrossRef](#)] [[PubMed](#)]
47. Chafie, M.; Ben Aissa, M.F.; Guizani, A. Energetic End Exergetic Performance of a Parabolic Trough Collector Receiver: An Experimental Study. *J. Clean. Prod.* **2018**, *171*, 285–296. [[CrossRef](#)]
48. Cao, F.; Wei, Q.; Liu, H.; Lu, N.; Zhao, L.; Guo, L. Development of the Direct Solar Photocatalytic Water Splitting System for Hydrogen Production in Northwest China: Design and Evaluation of Photoreactor. *Renew. Energy* **2018**, *121*, 153–163. [[CrossRef](#)]
49. Basem, A.; Moawed, M.; Abbood, M.H.; El-Maghlany, W.M. The Energy and Exergy Analysis of a Combined Parabolic Solar Dish—Steam Power Plant. *Renew. Energy Focus* **2022**, *41*, 55–68. [[CrossRef](#)]
50. Salamat, S.; Younesi, H.; Bahramifar, N. Synthesis of Magnetic Core-Shell Fe<sub>3</sub>O<sub>4</sub>@TiO<sub>2</sub> Nanoparticles from Electric Arc Furnace Dust for Photocatalytic Degradation of Steel Mill Wastewater. *RSC Adv.* **2017**, *7*, 19391–19405. [[CrossRef](#)]
51. Ung-Medina, F.; Caudillo-Flores, U.; Correa-González, J.C.; Maya-Yescas, R.; Chávez-Parga, M.D.C.; Cortés, J.A. Use of an Annular Non-Sleeve Photoreactor for Photocatalytic Dye Degradation: Study of Temperature and Light Intensity Effects. *Environ. Prog. Sustain. Energy* **2017**, *36*, 1083–1088. [[CrossRef](#)]
52. Wang, H.; Sun, Y.; Wu, Y.; Tu, W.; Wu, S.; Yuan, X.; Zeng, G.; Xu, Z.J.; Li, S.; Chew, J.W. Electrical Promotion of Spatially Photoinduced Charge Separation via Interfacial-Built-in Quasi-Alloying Effect in Hierarchical Zn<sub>2</sub>In<sub>2</sub>S<sub>5</sub>/Ti<sub>3</sub>C<sub>2</sub>(O, OH)<sub>x</sub> Hybrids toward Efficient Photocatalytic Hydrogen Evolution and Environmental Remediation. *Appl. Catal. B Environ.* **2019**, *245*, 290–301. [[CrossRef](#)]
53. Liu, B.; Wu, H.; Parkin, I.P. New Insights into the Fundamental Principle of Semiconductor Photocatalysis. *ACS Omega* **2020**, *5*, 14847–14856. [[CrossRef](#)]
54. Herrmann, J.M. Heterogeneous Photocatalysis: State of the Art and Present Applications In honor of Pr. R.L. Burwell Jr. (1912–2003), Former Head of Ipatieff Laboratories, Northwestern University, Evanston (Ill). *Top. Catal.* **2005**, *34*, 49–65. [[CrossRef](#)]
55. Al-Soud, M.S.; Hrayshat, E.S. A 50 MW Concentrating Solar Power Plant for Jordan. *J. Clean. Prod.* **2009**, *17*, 625–635. [[CrossRef](#)]
56. Balzar, A.; Stumpf, P.; Eckhoff, S.; Ackermann, H.; Grupp, M. A Solar Cooker Using Vacuum-Tube Collectors with Integrated Heat Pipes. *Sol. Energy* **1996**, *58*, 63–68. [[CrossRef](#)]
57. Jafari Mosleh, H.; Mamouri, S.J.; Shafii, M.B.; Hakim Sima, A. A New Desalination System Using a Combination of Heat Pipe, Evacuated Tube and Parabolic through Collector. *Energy Convers. Manag.* **2015**, *99*, 141–150. [[CrossRef](#)]
58. Abu-Hamdeh, N.H.; Alnefaie, K.A.; Almitani, K.H. Design and Performance Characteristics of Solar Adsorption Refrigeration System Using Parabolic Trough Collector: Experimental and Statistical Optimization Technique. *Energy Convers. Manag.* **2013**, *74*, 162–170. [[CrossRef](#)]
59. Bigoni, R.; Kötzsch, S.; Sorlini, S.; Egli, T. Solar Water Disinfection by a Parabolic Trough Concentrator (PTC): Flow-Cytometric Analysis of Bacterial Inactivation. *J. Clean. Prod.* **2014**, *67*, 62–71. [[CrossRef](#)]
60. Fernandez-Ibañez, P.; Malato, S.; Enea, O. Photoelectrochemical Reactors for the Solar Decontamination of Water. *Catal. Today* **1999**, *54*, 329–339. [[CrossRef](#)]
61. García-Montaña, J.; Pérez-Estrada, L.; Oller, I.; Maldonado, M.I.; Torrades, F.; Peral, J. Pilot Plant Scale Reactive Dyes Degradation by Solar Photo-Fenton and Biological Processes. *J. Photochem. Photobiol. A Chem.* **2008**, *195*, 205–214. [[CrossRef](#)]
62. Fernández-García, A.; Rojas, E.; Pérez, M.; Silva, R.; Hernández-Escobedo, Q.; Manzano-Agugliaro, F. A Parabolic-Trough Collector for Cleaner Industrial Process Heat. *J. Clean. Prod.* **2015**, *89*, 272–285. [[CrossRef](#)]
63. Wu, S.Y.; Xiao, L.; Cao, Y.; Li, Y.R. A Parabolic Dish/AMTEC Solar Thermal Power System and Its Performance Evaluation. *Appl. Energy* **2010**, *87*, 452–462. [[CrossRef](#)]
64. El-Kassaby, M.M. New Solar Cooker of Parabolic Square Dish: Design and Simulation. *Renew. Energy* **1991**, *1*, 59–65. [[CrossRef](#)]
65. Grupp, M.; Balmer, M.; Beall, B.; Bergler, H.; Cieslok, J.; Hancock, D.; Schröder, G. On-Line Recording of Solar Cooker Use Rate by a Novel Metering Device: Prototype Description and Experimental Verification of Output Data. *Sol. Energy* **2009**, *83*, 276–279. [[CrossRef](#)]
66. Badran, A.A.; Yousef, I.A.; Joudeh, N.K.; Hamad, R.; Al Halawa, H.; Hassouneh, H.K. Portable Solar Cooker and Water Heater. *Energy Convers. Manag.* **2010**, *51*, 1605–1609. [[CrossRef](#)]
67. Srithar, K.; Rajaseenivasan, T.; Karthik, N.; Periyannan, M.; Gowtham, M. Stand Alone Triple Basin Solar Desalination System with Cover Cooling and Parabolic Dish Concentrator. *Renew. Energy* **2016**, *90*, 157–165. [[CrossRef](#)]
68. Imran Khan, M.; Asfand, F.; Al-Ghamdi, S.G. Progress in Technology Advancements for next Generation Concentrated Solar Power Using Solid Particle Receivers. *Sustain. Energy Technol. Assess.* **2022**, *54*, 102813. [[CrossRef](#)]
69. Wang, Q.; Yao, Y.; Shen, Z.; Hu, M.; Yang, H. Concentrated Solar Power Tower Systems Coupled Locally with Spectrally Selective Coatings for Enhancement of Solar-Thermal Conversion and Economic Performance. *Green Energy Resour.* **2023**, *1*, 100001. [[CrossRef](#)]
70. González-Mora, E.; Dolores Durán García, M. Methodology for an Opto-Geometric Optimization of a Linear Fresnel Reflector for Direct Steam Generation. *Energies* **2020**, *13*, 355. [[CrossRef](#)]

71. Sebastián, A.; Abbas, R.; Valdés, M.; Casanova, J. Innovative Thermal Storage Strategies for Fresnel-Based Concentrating Solar Plants with East-West Orientation. *Appl. Energy* **2018**, *230*, 983–995. [[CrossRef](#)]
72. Mills, D.R.; Morrison, G.L. Compact Linear Fresnel Reflector Solar Thermal Powerplants. *Sol. Energy* **2000**, *68*, 263–283. [[CrossRef](#)]
73. Ochoa-Gutiérrez, K.S.; Tabares-Aguilar, E.; Mueses, M.Á.; Machuca-Martínez, F.; Li Puma, G. A Novel Prototype Offset Multi Tubular Photoreactor (OMTP) for Solar Photocatalytic Degradation of Water Contaminants. *Chem. Eng. J.* **2018**, *341*, 628–638. [[CrossRef](#)]
74. Anderson, J.V.; Link, H.; Bohn, M.; Gupta, B. Development of Solar Detoxification Technology in the USA—An Introduction. *Sol. Energy Mater.* **1991**, *24*, 538–549. [[CrossRef](#)]
75. Minero, C.; Pelizzetti, E.; Malato, S.; Blanco, J. Large Solar Plant Photocatalytic Water Decontamination: Degradation of Pentachlorophenol. *Chemosphere* **1993**, *26*, 2103–2119. [[CrossRef](#)]
76. Malato, S.; Blanco, J.; Richter, C.; Curco, D.; Gimenez, J. Low-Concentrating CPC Collectors for Photocatalytic Water Detoxification: Comparison with a Medium Concentrating Solar Collector. *Water Sci. Technol.* **1997**, *35*, 157–164. [[CrossRef](#)]
77. Klare, M.; Scheen, J.; Vogelsang, K.; Jacobs, H.; Broekaert, J.A.C. Degradation of Short-Chain Alkyl- and Alkanolamines by TiO<sub>2</sub>- and Pt/TiO<sub>2</sub>-Assisted Photocatalysis. *Chemosphere* **2000**, *41*, 353–362. [[CrossRef](#)] [[PubMed](#)]
78. Sano, T.; Negishi, N.; Takeuchi, K.; Matsuzawa, S. Degradation of Toluene and Acetaldehyde with Pt-Loaded TiO<sub>2</sub> Catalyst and Parabolic Trough Concentrator. *Sol. Energy* **2004**, *77*, 543–552. [[CrossRef](#)]
79. Bandala, E.R.; Arancibia-Bulnes, C.A.; Orozco, S.L.; Estrada, C.A. Solar Photoreactors Comparison Based on Oxalic Acid Photocatalytic Degradation. *Sol. Energy* **2004**, *77*, 503–512. [[CrossRef](#)]
80. McLoughlin, O.A.; Kehoe, S.C.; McGuigan, K.G.; Duffy, E.F.; Al Touati, F.; Gernjak, W.; Oller Alberola, I.; Malato Rodríguez, S.; Gill, L.W. Solar Disinfection of Contaminated Water: A Comparison of Three Small-Scale Reactors. *Sol. Energy* **2004**, *77*, 657–664. [[CrossRef](#)]
81. Barzegar, M.H.; Sabzehmeidani, M.M.; Ghaedi, M.; Avargani, V.M.; Moradi, Z.; Roy, V.A.L.; Heidari, H. S-Scheme Heterojunction g-C<sub>3</sub>N<sub>4</sub>/TiO<sub>2</sub> with Enhanced Photocatalytic Activity for Degradation of a Binary Mixture of Cationic Dyes Using Solar Parabolic Trough Reactor. *Chem. Eng. Res. Des.* **2021**, *174*, 307–318. [[CrossRef](#)]
82. Oyama, T.; Aoshima, A.; Horikoshi, S.; Hidaka, H.; Zhao, J.; Serpone, N. Solar Photocatalysis, Photodegradation of a Commercial Detergent in Aqueous TiO<sub>2</sub> Dispersions under Sunlight Irradiation. *Sol. Energy* **2004**, *77*, 525–532. [[CrossRef](#)]
83. Ma, R.; Su, H.; Sun, J.; Li, D.; Zhang, Z.; Wei, J. Concentrating Photo-Thermo-Organized Single-Atom and 2D-Raft Cu Catalyst for Full-Spectrum Solar Harmonic Conversion of Aqueous Urea and Urine into Hydrogen. *Appl. Catal. B Environ.* **2022**, *315*, 121493. [[CrossRef](#)]
84. Vidal, A.; Díaz, A.I.; El Hraiki, A.; Romero, M.; Muguruza, I.; Senhaji, F.; González, J. Solar Photocatalysis for Detoxification and Disinfection of Contaminated Water: Pilot Plant Studies. *Catal. Today* **1999**, *54*, 283–290. [[CrossRef](#)]
85. Kositzki, M.; Poullos, I.; Malato, S.; Caceres, J.; Campos, A. Solar Photocatalytic Treatment of Synthetic Municipal Wastewater. *Water Res.* **2004**, *38*, 1147–1154. [[CrossRef](#)] [[PubMed](#)]
86. Fernández, P.; Blanco, J.; Sichel, C.; Malato, S. Water Disinfection by Solar Photocatalysis Using Compound Parabolic Collectors. *Catal. Today* **2005**, *101*, 345–352. [[CrossRef](#)]
87. Augugliaro, V.; García-López, E.; Loddo, V.; Malato-Rodríguez, S.; Maldonado, I.; Marci, G.; Molinari, R.; Palmisano, L. Degradation of Lincomycin in Aqueous Medium: Coupling of Solar Photocatalysis and Membrane Separation. *Sol. Energy* **2005**, *79*, 402–408. [[CrossRef](#)]
88. Villén, L.; Manjón, F.; García-Fresnadillo, D.; Orellana, G. Solar Water Disinfection by Photocatalytic Singlet Oxygen Production in Heterogeneous Medium. *Appl. Catal. B Environ.* **2006**, *69*, 1–9. [[CrossRef](#)]
89. Sichel, C.; Tello, J.; de Cara, M.; Fernández-Ibáñez, P. Effect of UV Solar Intensity and Dose on the Photocatalytic Disinfection of Bacteria and Fungi. *Catal. Today* **2007**, *129*, 152–160. [[CrossRef](#)]
90. Alrousan, D.M.A.; Polo-López, M.I.; Dunlop, P.S.M.; Fernández-Ibáñez, P.; Byrne, J.A. Solar Photocatalytic Disinfection of Water with Immobilised Titanium Dioxide in Re-Circulating Flow CPC Reactors. *Appl. Catal. B Environ.* **2012**, *128*, 126–134. [[CrossRef](#)]
91. Quiñones, D.H.; Álvarez, P.M.; Rey, A.; Beltrán, F.J. Removal of Emerging Contaminants from Municipal WWTP Secondary Effluents by Solar Photocatalytic Ozonation. A Pilot-Scale Study. *Sep. Purif. Technol.* **2015**, *149*, 132–139. [[CrossRef](#)]
92. Colina-Márquez, J.; Machuca-Martínez, F.; Puma, G.L. Modeling the Photocatalytic Mineralization in Water of Commercial Formulation of Estrogens 17-β Estradiol (E2) and Noregestrol Acetate in Contraceptive Pills in a Solar Powered Compound Parabolic Collector. *Molecules* **2015**, *20*, 13354–13373. [[CrossRef](#)]
93. Otálvaro-Marín, H.L.; Mueses, M.A.; Crittenden, J.C.; Machuca-Martínez, F. Solar Photoreactor Design by the Photon Path Length and Optimization of the Radiant Field in a TiO<sub>2</sub>-Based CPC Reactor. *Chem. Eng. J.* **2017**, *315*, 283–295. [[CrossRef](#)]
94. Aguas, Y.; Hincapie, M.; Fernández-Ibáñez, P.; Polo-López, M.I. Solar Photocatalytic Disinfection of Agricultural Pathogenic Fungi (*Curvularia* Sp.) in Real Urban Wastewater. *Sci. Total Environ.* **2017**, *607–608*, 1213–1224. [[CrossRef](#)] [[PubMed](#)]
95. Haranaka-Funai, D.; Didier, F.; Giménez, J.; Marco, P.; Esplugas, S.; Machulek-Junior, A. Photocatalytic Treatment of Valproic Acid Sodium Salt with TiO<sub>2</sub> in Different Experimental Devices: An Economic and Energetic Comparison. *Chem. Eng. J.* **2017**, *327*, 656–665. [[CrossRef](#)]

96. Moreira, N.F.F.; Narciso-da-Rocha, C.; Polo-López, M.I.; Pastrana-Martínez, L.M.; Faria, J.L.; Manaia, C.M.; Fernández-Ibáñez, P.; Nunes, O.C.; Silva, A.M.T. Solar Treatment (H<sub>2</sub>O<sub>2</sub>, TiO<sub>2</sub>-P<sub>25</sub> and GO-TiO<sub>2</sub> Photocatalysis, Photo-Fenton) of Organic Micropollutants, Human Pathogen Indicators, Antibiotic Resistant Bacteria and Related Genes in Urban Wastewater. *Water Res.* **2018**, *135*, 195–206. [[CrossRef](#)]
97. López, N.; Marco, P.; Giménez, J.; Esplugas, S. Photocatalytic Diphenhydramine Degradation under Different Radiation Sources: Kinetic Studies and Energetic Comparison. *Appl. Catal. B Environ.* **2018**, *220*, 497–505. [[CrossRef](#)]
98. Vela, N.; Calín, M.; Yáñez-Gascón, M.J.; Garrido, I.; Pérez-Lucas, G.; Fenoll, J.; Navarro, S. Solar Reclamation of Wastewater Effluent Polluted with Bisphenols, Phthalates and Parabens by Photocatalytic Treatment with TiO<sub>2</sub>/Na<sub>2</sub>S<sub>2</sub>O<sub>8</sub> at Pilot Plant Scale. *Chemosphere* **2018**, *212*, 95–104. [[CrossRef](#)]
99. Luna-Sanguino, G.; Ruíz-Delgado, A.; Tolosana-Moranchel, A.; Pascual, L.; Malato, S.; Bahamonde, A.; Faraldos, M. Solar Photocatalytic Degradation of Pesticides over TiO<sub>2</sub>-RGO Nanocomposites at Pilot Plant Scale. *Sci. Total Environ.* **2020**, *737*, 140286. [[CrossRef](#)]
100. Zheng, Q.; Aiello, A.; Choi, Y.S.; Tarr, K.; Shen, H.; Durkin, D.P.; Shuai, D. 3D Printed Photoreactor with Immobilized Graphitic Carbon Nitride: A Sustainable Platform for Solar Water Purification. *J. Hazard. Mater.* **2020**, *399*, 123097. [[CrossRef](#)]
101. Minero, C.; Pelizzetti, E.; Malato, S.; Blanco, J. Large Solar Plant Photocatalytic Water Decontamination: Degradation of Atrazine. *Sol. Energy* **1996**, *56*, 411–419. [[CrossRef](#)]
102. Malato, S.; Blanco, J.; Vidal, A.; Richter, C. Photocatalysis with Solar Energy at a Pilot-Plant Scale: An Overview. *Appl. Catal. B Environ.* **2002**, *37*, 1–15. [[CrossRef](#)]
103. Cao, F.; Pang, J.; Gu, X.; Wang, M.; Shangguan, Y. Performance Simulation of Solar Trough Concentrators: Optical and Thermal Comparisons. *Energies* **2023**, *16*, 1673. [[CrossRef](#)]
104. Mussard, M.; Nydal, O.J. Charging of a Heat Storage Coupled with a Low-Cost Small-Scale Solar Parabolic Trough for Cooking Purposes. *Sol. Energy* **2013**, *95*, 144–154. [[CrossRef](#)]
105. Stanek, B.; Wećel, D.; Bartela, Ł.; Rulik, S. Solar Tracker Error Impact on Linear Absorbers Efficiency in Parabolic Trough Collector—Optical and Thermodynamic Study. *Renew. Energy* **2022**, *196*, 598–609. [[CrossRef](#)]
106. Beltran, R.; Velazquez, N.; Espericueta, A.C.; Saucedo, D.; Perez, G. Mathematical Model for the Study and Design of a Solar Dish Collector with Cavity Receiver for Its Application in Stirling Engines. *J. Mech. Sci. Technol.* **2012**, *26*, 3311–3321. [[CrossRef](#)]
107. Nepveu, F.; Ferriere, A.; Bataille, F. Thermal Model of a Dish/Stirling Systems. *Sol. Energy* **2009**, *83*, 81–89. [[CrossRef](#)]
108. El Ouederni, A.R.; Salah, M.B.; Askri, F.; Nasrallah, M.B.; Aloui, F. Experimental Study of a Parabolic Solar Concentrator. *J. Renew. Energ.* **2009**, *12*, 395–404.
109. Abbas, R.; Montes, M.J.; Piera, M.; Martínez-Val, J.M. Solar Radiation Concentration Features in Linear Fresnel Reflector Arrays. *Energy Convers. Manag.* **2012**, *54*, 133–144. [[CrossRef](#)]
110. Geyer, M.; Lüpfert, E.; Osuna, R.; Nava, P.; Langenkamp, J.; Mandelberg, E. EUROTROUGH-Parabolic Trough Collector Developed for Cost Efficient Solar Power Generation. In Proceedings of the 11th International Symposium on Concentrating Solar Power and Chemical Energy Technologies, Zurich, Switzerland, 4–6 September 2002; Volume 7.
111. Sharma, A.K.; Sharma, C.; Mullick, S.C.; Kandpal, T.C. GHG Mitigation Potential of Solar Industrial Process Heating in Producing Cotton Based Textiles in India. *J. Clean. Prod.* **2017**, *145*, 74–84. [[CrossRef](#)]
112. Palenzuela, P.; Zaragoza, G.; Alarcón-Padilla, D.C.; Guillén, E.; Ibarra, M.; Blanco, J. Assessment of Different Configurations for Combined Parabolic-Trough (PT) Solar Power and Desalination Plants in Arid Regions. *Energy* **2011**, *36*, 4950–4958. [[CrossRef](#)]
113. Peiró, G.; Prieto, C.; Gasia, J.; Jové, A.; Miró, L.; Cabeza, L.F. Two-Tank Molten Salts Thermal Energy Storage System for Solar Power Plants at Pilot Plant Scale: Lessons Learnt and Recommendations for Its Design, Start-up and Operation. *Renew. Energy* **2018**, *121*, 236–248. [[CrossRef](#)]
114. de Risi, A.; Milanese, M.; Laforgia, D. Modelling and Optimization of Transparent Parabolic Trough Collector Based on Gas-Phase Nanofluids. *Renew. Energy* **2013**, *58*, 134–139. [[CrossRef](#)]
115. Linares, J.I.; Montes, M.J.; Cantizano, A.; Sánchez, C. A Novel Supercritical CO<sub>2</sub> Recompression Brayton Power Cycle for Power Tower Concentrating Solar Plants. *Appl. Energy* **2020**, *263*, 114644. [[CrossRef](#)]
116. Zhuang, X.; Wang, H.; Lu, H.; Yang, Z.; Guo, H. Numerical Investigation of Heat Transfer and Flow Characteristics of Supercritical CO<sub>2</sub> in Solar Tower Microchannel Receivers at High Temperature. *Energies* **2023**, *16*, 6445. [[CrossRef](#)]
117. Pino, F.J.; Caro, R.; Rosa, F.; Guerra, J. Experimental Validation of an Optical and Thermal Model of a Linear Fresnel Collector System. *Appl. Therm. Eng.* **2013**, *50*, 1463–1471. [[CrossRef](#)]
118. Beltagy, H.; Semmar, D.; Lehaut, C.; Said, N. Theoretical and Experimental Performance Analysis of a Fresnel Type Solar Concentrator. *Renew. Energy* **2017**, *101*, 782–793. [[CrossRef](#)]
119. Mills, D.R.; Morrison, G.L. Modelling Study for Compact Fresnel Reflector Power Plant. *Le J. De Phys. IV* **1999**, *9*, Pr3-159–Pr3-165. [[CrossRef](#)]

**Disclaimer/Publisher's Note:** The statements, opinions and data contained in all publications are solely those of the individual author(s) and contributor(s) and not of MDPI and/or the editor(s). MDPI and/or the editor(s) disclaim responsibility for any injury to people or property resulting from any ideas, methods, instructions or products referred to in the content.